To the Graduate Council:

I am submitting herewith a thesis written by Chang-Uk Lee entitled "Controlling the Dispersion of Nanoparticles in Polymer Matrices." I have examined the final paper copy of this thesis for form and content and recommend that it be accepted in partial fulfillment of the requirements for the degree of Master of Science, with a major in Polymer Engineering.

Mark Dadmun, Major Professor

We have read this thesis
and recommend its acceptance:

Jimmy Mays

Kevin Kit

Accepted for the Council:

Interim Dean of Graduate Studies

Thesis
2006
.L36

CONTROLLING THE DISPERSION OF NANOPARTICLES IN POLYMER MATRICES

A Thesis

Presented for the

Master of Science Degree

The University of Tennessee, Knoxville

Chang-Uk Lee

December 2006

ACKNOWLEDGEMENT

I would first like to thank my parents, Byung-Mun Lee and Jeong-Ja Do, for their endless love and support. I would like to thank my sisters, Kyung-Mi, Sun-Hwa, and Kyung-A, who always give me confidence.

I would like to thank my advisor, Professor Mark Dadmun, for his leadership, intelligence, and help to make this research possible. I would like to thank my committee members, Professor Jimmy Mays and Professor Kevin Kit, for their time and assistance. I would like to thank my lab members, Rujul Mehta, Sudesh Kamath, Zhenyu Huang, Nathan Crawford, Kevin Rice, Asif Rasheed, Michael Lay, Nathan Henry, Deepali Kumar, Earl Ashcraft, Shraddha Deodhar, Brian Bachner, Caleb Dyer, and Diaz Linton, for their camaraderie and discussions during this research.

I would like to thank Professor Kevin Kit for helpful discussions regarding DMA sample preparation. I would like to thank Professor Jimmy Mays and Haining Ji for helpful discussions regarding PSVPh-SH synthesis. Special thanks to Deepali Kumar for teaching me polymer synthesis.

This research was financially supported by NSF through grants DMR 0241214 and CRC-Chem-0304807.

ABSTRACT

The dispersion of nanoparticles in a polymer matrix is a critical parameter to design and realize targeted morphologies and properties of a final polymer-based nanocomposite. This thesis presents experimental studies to investigate the dispersion of nanoparticles in polymer matrices using specific intermolecular hydrogen bonding between the nanoparticles and polymer matrices under two main topics.

The first topic is the impact of sample preparation processes on the properties of polymer carbon nanotube nanocomposites. Polymer nanocomposites composed of poly(styrene-co-vinyl phenol) (PSVPh) copolymers and 5 wt % multi-walled carbon nanotubes (MWNTs) were prepared from three different methods, including melt-mixing and solution casting. The MWNTs were either oxidized to incorporate oxygenated defects or utilized as received. The mechanical properties of the nanocomposites were measured by DMA, and the extent of intermolecular hydrogen bonding between MWNTs and PSVPh was quantified by IR. Our DMA results suggest that melt-mixing leads to more stable morphologies of the final nanocomposites than solution casting does. Additionally, the IR analysis of the nanocomposites indicates melt-mixing can result in the formation of more intermolecular hydrogen bonding between the MWNTs and PSVPh than solution casting, and thus suggests that melt-mixing leads to more reproducible mechanical properties than solution casting. Our DMA and IR results may provide guidelines to realize the desired morphologies and to improve the properties of polymer carbon nanotube nanocomposites by optimizing intermolecular interactions between MWNTs and polymers.

The other topic examined seeks to synthesize the starting materials to sequester

surface-modified gold nanoparticles in a diblock copolymer matrix. The long term goal of this project is to investigate the impact of enthalpic attractions between the gold nanoparticles and one phase of the diblock copolymer on the nanocomposite morphologies. That is, this system is designed such that the hydroxyl groups on the gold nanoparticles can hydrogen bond with poly(2-vinyl pyridine) blocks of poly(styrene-b-2-vinyl pyridine) diblock copolymers. Polystyrene-coated gold nanoparticles were synthesized using thiol-terminated polystyrene (PS-SH) as a stabilizing ligand. The low molecular weight PS-SH was obtained by the thiolation of bromine-terminated polystyrene (PS-Br), which was synthesized by ATRP. TEM images of the gold nanoparticles shows that the size of the gold nanoparticles can be controlled using this PS-SH as a stabilizing ligand. Additionally, the synthesis of thiol-terminated poly(styrene-co-vinyl phenol) (PSVPh-SH) copolymers was attempted starting with bromine-terminated poly(styrene-co-4-tert-butoxystyrene) copolymers, followed by thiolation and hydrolysis. Our NMR results indicate that the conversion of the bromine-end groups of the copolymers to thiol-end groups by thiolation was complete. However, the conversion of the tert-butoxy groups of the thiolated copolymers to hydroxyl groups by hydrolysis using HCl was not successful. Furthermore, NMR data suggests that this hydrolysis may impact the thiol-end groups of the thiol-terminated copolymers. Our NMR results may provide guidelines such that carefully controlled reaction time and/or HCl amount would improve the success of the PSVPh-SH synthesis.

TABLE OF CONTENTS

CHAPTER 1 1

INTRODUCTION 1

1.1 Dispersion of Nanoparticles in Polymer Matrices: Introduction and Literature Review 1

1.2 The Impact of Sample Preparation on Polymer Carbon Nanotube Nanocomposites 6

1.2.1 Carbon Nanotubes as a Filler 6

1.2.2 Chemical Functionalization of CNTs 9

1.2.3 Nanocomposite Preparation Processes 11

1.3 Sequestering Surface-modified Gold Nanoparticles in Diblock Copolymers: Starting Materials 14

CHAPTER 2 19

THE IMPACT OF SAMPLE PREPARATION ON POLYMER CARBON NANOTUBE NANOCOMPOSITES 19

2.1 Experimental 19

2.1.1 Synthesis of Poly(styrene-co-vinyl phenol) (PSVPh) 19

2.1.2 Oxidation of Multi-walled Carbon Nanotubes and Raman Spectroscopy of MWNTs 20

2.1.3 Preparation of Nanocomposites 23

2.1.4 Dynamic Mechanical Analysis (DMA) 26

2.1.5 Infrared (IR) Spectroscopy 27

2.1.6 Raman Spectroscopy and Scanning Electron Microscopy 28

2.2 Results and Discussion 28

2.2.1 PSVPh Copolymer Characterization 28

2.2.2 Characterization of MWNTs 31

2.2.3 Dynamic Mechanical Analysis 34

2.2.4 Infrared Spectroscopy of Nanocomposites: Correlate Mechanical Properties with Intermolecular Interactions 47

2.3 Conclusions 59

CHAPTER 3 60

SEQUESTERING SURFACE-MODIFIED GOLD NANOPARTICLES IN DIBLOCK COPOLYMERS: STARTING MATERIALS 60

3.1 Experimental 60

3.1.1 Synthesis of Thiol-terminated Polystyrene 60

3.1.2 Synthesis of Polystyrene-coated Gold Nanoparticles 61

3.1.3 Transmission Electron Microscopy (TEM) of Gold Nanoparticles 63

3.1.4 Synthesis of Bromine-terminated Poly(styrene-co-acetoxystyrene) Copolymers, and their Hydrolysis or Thiolation 64

3.1.5 Synthesis of Thiol-terminated Poly(styrene-co-vinyl phenol) Copolymers 65

3.2 Results and Discussion 68

3.2.1 Bromine-terminated Polystyrene 68

3.2.2 Thiol-terminated Polystyrene 70

3.2.3 Polystyrene-coated Gold Nanoparticles 70

3.2.4 Attempt for Synthesis of Thiol-terminated Poly(styrene-co-vinyl phenol) Copolymers Starting with Bromine-terminated Poly(styrene-co-acetoxystyrene) Copolymers 73

3.2.5 Bromine-terminated Poly(styrene-co-4-tert-butoxystyrene) Copolymers 78

3.2.6 Thiol-terminated Poly(styrene-co-4-tert-butoxystyrene) Copolymers 78

3.2.7 Hydrolysis of Thiol-terminated Poly(styrene-co-tert-butoxystyrene) Copolymers 80

3.3 Conclusions 84

CHAPTER 4 86

CONCLUSIONS AND FUTURE WORK 86

LIST OF REFERENCES 92

VITA 97

LIST OF TABLES

Table 2.1 Summary of Raman spectroscopy of MWNTs treated with various oxidizing agents or untreated MWNTs. 33

Table 2.2 Summary of peak-fitting results for nanocomposites from three different sample preparation procedures. 55

LIST OF FIGURES

Figure 2.1 Scheme of synthesis procedure for PSVPh copolymers..... 21

Figure 2.2 Scheme of sample preparation processes for polymer carbon nanotube nanocomposites. MM: Melt-Mixing process, SCM: Solution-Casting after Melt-mixing, and SCD: Solution-Casting after Dissolving polymers in MWNT-DMF suspension..... 24

Figure 2.3 ^{1}H spectra of (a) poly(styrene-co-acetoxystyrene) copolymers and (b) poly(styrene-co-vinyl phenol) copolymers after hydrolysis. 30

Figure 2.4 Raman spectra of oxidized MWNTs from 4 different oxidation processes and unoxidized MWNTs..... 32

Figure 2.5 Representative SEM images of MWNTs. (a) unoxidized, (b) 6M nitric acid treated, and (c) 6M nitric acid and then piranha solution treated MWNTs. ... 35

Figure 2.6 Storage modulus of PSVPh samples prepared from MM (MM_PSVPh), SCM (SCM_PSVPh), or SCD (SCD_PSVPh) methods as a function of temperature. 38

Figure 2.7 Storage modulus ratio of MM nanocomposites with oxidized (◊) and unoxidized (x) MWNTs normalized to that of the PSVPh as a function of temperature (T – Tg). 39

Figure 2.8 Storage modulus ratio of SCM nanocomposites with oxidized and unoxidized MWNTs normalized to that of the PSVPh as a function of temperature (T – Tg)..... 41

Figure 2.9 Storage modulus ratio of SCD nanocomposites with oxidized and unoxidized MWNTs normalized to that of the PSVPh as a function of temperature (T –

Tg). 43

Figure 2.10 Storage modulus ratio of SCD_2nd samples with oxidized or unoxidized MWNTs to that of PSVPh as a function of temperature (T – Tg). 44

Figure 2.11 Storage modulus ratio of SCD&MM samples with oxidized or unoxidized MWNTs to that of PSVPh as a function of temperature (T – Tg). 46

Figure 2.12 Summary of storage modulus ratio of nanocomposites with oxidized MWNTs from MM, SCM, or SCD. 48

Figure 2.13 Summary of storage modulus ratio of nanocomposites with unoxidized MWNTs from MM, SCM, or SCD. 49

Figure 2.14 Scheme of possible O-H stretching vibrations in this study. 51

Figure 2.15 Example of peak-fitted curves of a MM_Oxidized nanocomposite 54

Figure 2.16 The ratio of concentration of free ($C_{F,OH}$), intra-associated ($C_{A,OH}$) and inter-associated ($C_{I,OH}$) to that of total OH ($C_{T,OH}$) vibration for nanocomposites with (a) oxidized and (b) unoxidized MWNTs. 56

Figure 2. 17 Storage modulus ratio (♦) of MM, SCM, or SCD samples with oxidized or unoxidized MWNTs normalized to that of the PSVPh as a function of the ratio of concentration of inter-associated ($C_{I,OH}$) to that of total OH ($C_{T,OH}$) vibration. 58

Figure 3.1 Scheme for synthesis procedure of PS-SH[48] 62

Figure 3.2 Scheme for synthesis procedures for thiol-terminated poly(styrene-co-vinyl phenol) copolymers starting with bromine-terminated poly(styrene-co-4-tert-

butoxystyrene) copolymers. 66

Figure 3.3 ^{1}H spectrum of bromine-terminated polystyrene dissolved in deuterated chloroform. 71

Figure 3.4 ^{1}H spectrum of thiol-terminated polystyrene dissolved in deuterated chloroform. 72

Figure 3.5 Representative TEM image of PS-coated gold nanoparticles. (Scale bar size: 100 nm) 74

Figure 3.6 Size and size distribution of PS-coated gold nanoparticles. 75

Figure 3.7 ^{1}H spectrum of bromine-terminated poly(styrene-co-4-tert-butoxystyrene) copolymers dissolved in deuterated dioxane. 79

Figure 3.8 ^{1}H spectrum of thiol-terminated poly(styrene-co-tert-butoxystyrene) copolymers dissolved in deuterated chloroform. 81

Figure 3.9 ^{1}H NMR spectrum of thiol-terminated poly(styrene-co-4-tert-butoxystyrene) copolymers dissolved in deuterated chloroform after hydrolysis. 82

Figure 4.1 Scheme of future work for sequestering surface-modified gold nanoparticles in diblock copolymers. 91

CHAPTER 1
INTRODUCTION

1.1 Dispersion of Nanoparticles in Polymer Matrices: Introduction and Literature Review

Recently, polymer-based nanocomposites composed of polymers and nano-size fillers[1] have been an important research area in polymer science and engineering in that the creation of these nanocomposites makes it possible to utilize the mechanical, optical, or conductive properties of metal or semiconductor nanoparticles within polymer matrices.[2-4] Widely used nanoscale fillers include carbon nanotubes, clays, and metal nanoparticles[5], which are classified as nanoparticles in this thesis. The utilization of nanoparticles in polymer-based composites has been motivated by several advantages compared to the conventional micro-size fillers.[6] One of the advantages can be to maximize the efficiency of fillers by increasing interfacial area per particle volume as nano-size fillers with large surface-area-to-volume ratios are involved in nanocomposites. Bockstaller et al.[6] demonstrated that the interfacial area per particle volume can increase from 10^{-4} for micro-size fillers such as glass fibers to 10^{-1} for nano-size fillers such as clay and spherical nanoparticles. Furthermore, the specific properties of polymeric materials can be improved while other properties remain unchanged.[1,6] For example, Kawasumi et al.[7] reported the improvement of the heat-distortion property and storage modulus above Tg of clay-nylon-6 nanocomposites. Specifically, the storage modulus at 120 °C of the nanocomposite with 5 wt % clay increase by three times relative to that of the neat nylon-6. However, they showed that the nano-size clays in the polymer matrix

did not impact the transparency of the nylon-6 film.

Various types of polymers have been used as a matrix, such as homopolymers, random polymers, and block copolymers, to attempt to tailor nanocomposite morphologies, which may impact the properties of the nanocomposites. Nanoparticles are generally incorporated into homopolymers with the main purpose of improving the mechanical or thermal properties of the polymers.[6] For examples, Okada et al.[8] reported the formation of nylon-6/clay nanocomposites with improvement of the tensile strength (from 69 to 107 MPa) and the tensile modulus (from 1.1 to 2.1 GPa) with 4.2 wt % clays relative to that of nylon 6. This study shows that homogeneously dispersed clays in homopolymers can lead to improved mechanical properties of nanocomposites.

Additionally, block copolymers, "which are macromolecules composed of sequences, or blocks, of chemically distinct repeat units"[9], have attracted many researchers' attention as a polymer matrix in nanocomposites in that the microphase separation of block copolymers can lead to highly ordered morphologies, such as lamellae, hexagonally packed cylinder, and body-centered cubic sphere structures by self-assembly processes.[9-11] For example, Sita and co-workers[12] reported the selective dispersion of alkanethiol-passivated gold nanoparticles into the polystyrene blocks of poly(styrene-b-methyl methacrylate), PS-b-PMMA, diblock copolymers, which microphase-separated into lamellar phases. In this work, chemical compatibility between the non-polar alkanethiol-coated gold nanoparticles and non-polar PS domains and chemical incompatibility between the gold nanoparticles and the polar PMMA domains led to the selective dispersion of the gold nanoparticles into the PS blocks. As a result, the alkanethiol-coated gold nanoparticles were localized in the PS-domains. This study

suggests that nanocomposites with ordered morphologies can be formed by sequestering surface-modified gold nanoparticles in a diblock copolymer matrix.

However, the control and manipulation of the dispersion of nanoparticles in a polymer matrix is important in order to design and realize tailored morphologies of final polymer-based nanocomposites and to optimize the properties of nanocomposites. Important parameters for the dispersion of nanoparticles include the control of intermolecular interactions between nanoparticles and polymer matrices, and the characteristics of nanoparticles. First, it is possible to control the dispersion of nanoparticles by incorporating intermolecular interactions between nanoparticles and a polymer matrix. Chemical functionalization of either nanoparticles or polymer matrices can be a useful way to induce intermolecular interactions. One way of chemical functionalization of nanoparticles is to graft short-chain polymers or functional groups on the surface of nanoparticles. For example, Boal et al.[13] developed three points of hydrogen bonding between thymine-functionalized gold nanoparticles and diaminotriazine-functionalized polystyrene to create the aggregates of the particles and polymers. In this study, hydrogen bonding led to the formation of spherical aggregates of particles and polymers. This result suggests that hydrogen bonding can be used to control the dispersion and to form tailored morphologies in nanocomposites.

Second, the characteristics of nanoparticles can be an important factor to control the dispersion of nanoparticles and to determine the final morphologies of nanocomposites, especially when the nanoparticles are incorporated into diblock copolymers as a matrix. More specifically, the size and volume fraction of nanoparticles impacts the placement and loading of the particle in diblock copolymer nanocomposites.[4]

For example, Thomas and co-workers[14] prepared nanocomposites composed of poly(styrene-b-ethylene propylene) (PS-PEP) diblock copolymers, which form lamellar phases upon microphase separation, and gold or silica nanoparticles, which have diameters of 3.5 nm and 21.5 nm, respectively. The final morphology of the nanocomposites had the large silica particles located at the center of PEP domains, and small gold nanoparticles dispersed at the interface of PEP and PS domains. This experimental result suggests that the dispersion of nanoparticles in a diblock copolymer matrix can be manipulated by the size of the nanoparticle.

The controlled dispersion of nanoparticles can lead to tailored structures of nanocomposites, and thus result in a material that is useful in specific applications of nanocomposites, including chemical sensors and catalysts.[15] For example, one dimensional structures of particles in a polymer matrix leads to a system that can be utilized as chemical sensors, in which metal nanoparticles play the role as a provider of electrical conductivity, and the polymers act as chemical sensors with variable interparticle distances and interaction sites[2] . Krasteva et al.[2] developed chemical sensors composed of gold nanoparticles and three kinds of dendrimers, which were hydrophobic polyphenylene (PPh) dendrimer, hydrophilic poly(amidoamine) (PAMAM) dendrimers, and amphiphilic poly(propylene imine) (PPI) dendrimers. Each film of the Au/dendrimer nanocomposites was tested as a chemical sensor by dosing with vapors of toluene, 1-propanol, or water. Au/PPh sensors showed the highest resistance when exposed to toluene vapor, Au/PAMAM with 1-propanol, and Au/PPI with water. The increased resistance results from the increase of interparticle distances as dendrimers absorb analyte vapor and swell the polymer chains. This result shows specific morphologies with the

dispersed nanoparticles in polymers can lead to specific nanocomposite applications.

Additionally, the aggregate structures of nanoparticle-polymer composites suggest that they may be good catalysts.[16] As large surface areas are demanded for catalysts, nanoparticles in a polymer matrix are a good candidate to be used to create such systems.[15] Galow et al.[16] developed aggregates of acid-functionalized Pd and SiO_2 nanoparticles with amine-functionalized polymers as the precursor of catalysts. After calcination of the nanocomposite at 500 ^{o}C, highly porous catalysts were obtained. Their study suggests that nanoparticle-polymer nanocomposites can be fabricated into highly porous materials, which have the potential to behave as useful as catalysts.

In this study, experimental efforts to design tailored morphologies of polymer-based nanocomposites and to optimize their properties using specific intermolecular interactions between nanoparticles and polymer matrices were attempted with two different types of polymer nanocomposites. First, the morphologies of nanocomposites composed of multi-walled carbon nanotubes (MWNTs) and poly(styrene-co-vinyl phenol) (PSVPh) random copolymers were studied by investigating the mechanical properties of the nanocomposites prepared by different sample preparation processes. Also, the impact of intermolecular interactions between the MWNTs and PSVPh on the mechanical properties of the polymer nanocomposites was investigated. The MWNTs were chemically modified to incorporate intermolecular hydrogen bonding with the polymer matrix, or utilized as received. Additionally, the synthesis of the starting materials to sequester surface-modified gold nanoparticles in a diblock copolymer matrix was studied to investigate the impact of intermolecular interactions between the gold nanoparticles and diblock copolymer on the final morphologies of the diblock copolymer

nanocomposites. The synthesis of thiol-terminated short chain polymers to graft on gold nanoparticle surfaces were attempted to incorporate specific intermolecular hydrogen bonding between the surface-modified gold nanoparticles and one block of the diblock copolymer matrix.

1.2 The Impact of Sample Preparation on Polymer Carbon Nanotube Nanocomposites

1.2.1 Carbon Nanotubes as a Filler

Since their report in 1991[17], carbon nanotubes (CNTs) have attracted many researchers' attention due to their superior mechanical, optical, electrical, and thermal properties.[18] Two common CNTs are single-walled carbon nanotubes (SWNTs) and multi-walled carbon nanotubes (MWNTs): A SWNT is a hollow and cylindrical structure that is essentially a rolled up graphite sheet, and a MWNT is more than two SWNTs that are coaxial along a single hollow axis, in which the gap between tubes is generally around 0.34 nm.[18,19] CNTs have tubular structures of hexagonal network (defect-free nanotubes), and can also have structures of pentagon or heptagon defects, in which carbon atoms have sp^2 hybridized structures with in-plane σ bonding and out-of-plane π bonding.[18] Diameter of SWNTs typically ranges from 0.6 – 2 nm, and typical inner diameter of MWNTs is greater than 2 nm and outer diameter is less than 100 nm[18]. Length of CNTs ranges up to millimeters.[20] This ratio of length (l) to diameter (d) results in high aspect ratio (l/d) of CNTs. The typical density of CNTs is around 1.3 g/cm^3.[20]

Due to the extraordinary mechanical properties, low density, and high aspect ratio, CNTs are a good candidate as a filler for polymer nanocomposites to improve the

properties of polymeric materials. In theoretical[21,22] and experimental[23-26] studies, it has been shown that carbon nanotubes (CNTs) have extraordinary mechanical properties. First, theoretical studies estimate that the calculated Young's modulus of SWNTs is higher than 600 GPa. For example, Gao et al.[21] calculated Young's modulus of SWNTs by using molecular dynamics with the modulus in the range of 640 to 673 GPa.

Second, experimentally measured tensile modulus of CNTs has been reported as high as 1 TPa[19], with tensile strength up to 180 GPa.[19,27] These values indicates that CNTs have extraordinary mechanical properties when compared to the bulk modulus and strength of steel, which are 270 GPa and 1.4 GPa, respectively.[28] For example, Wong et al.[23] determined the Young's modulus of MWNTs by measuring the applied forces for bending a single nanotube and the displacement of the tube under forces. They fixed one end of a nanotube on cleaved MoS_2 substrate, and allowed the other end to bend as an atomic force microscope (AFM) tip moves the free end. By the analysis of bending forces and displacement of 6 nanotubes, they determined the Young's modulus of these MWNTs to be 1.28 +/- 0.59 TPa. In addition, Yu et al.[24] measured the mechanical properties of MWNTs by applying tensile stresses to the nanotubes. Due to the nano-size of the tubes, they attached each end of a single tube to opposite tips of an AFM, applied load to the tube, and investigated the deformation of tubes using scanning electron microscopy (SEM). In their work, the measured tensile strengths of 19 individual tubes ranged from 11 to 63 GPa. In addition, based on stress-strain analysis, the Young's modulus (E) of the tubes was in the range of 270 to 950 GPa.

However, when we incorporate CNTs into a polymer matrix, there can be two main barriers that must be overcome to utilize the superior properties of CNTs in a

polymer matrix.[29,30] First, CNTs can easily form aggregates or bundles due to van der Waals interactions among nanotubes.[29] The bundles of CNTs inhibit their solubility in organic or aqueous solvents, which may result in an inhomogeneous dispersion of CNTs in a polymer matrix[29]. Furthermore, the aggregation of CNTs decreases their aspect ratios, which reduces their efficiency as fillers.[29] Thus, the uniform and homogeneous dispersion of CNTs in a polymer matrix is required to optimize CNT nanocomposites.[29,30] Second, interactions between CNTs and polymer matrices may be weak, which leads to poor interfacial strength between CNTs and polymers.[29] These weak interactions can result in poor load transfer between CNTs to polymer matrices, and thus decrease their efficiency as fillers.[29] Therefore, strong interfacial interactions are also desired to create optimal CNT polymer nanocomposites.[29,30]

Many researchers have focused on developing methods to create uniform and homogenous dispersions of CNTs in polymer matrices and to enhance the interfacial strength of the CNT/polymer interface in an attempt to enhance the mechanical properties of CNT nanocomposites. Experimental efforts to improve dispersion of CNTs in nanocomposites include chemical functionalization of CNTs, which can lead to the incorporation of intermolecular interactions between CNTs and polymers, and understanding the role of sample preparation on the ultimate morphology and properties of polymer CNT nanocomposites.

1.2.2 Chemical Functionalization of CNTs

Chemical functionalization of CNTs refers to chemically modifying CNTs in order to incorporate functional groups on the surfaces.[19] Since intermolecular interactions between functionalized CNTs and a polymer matrix are possible, chemical functionalization has been widely utilized as a method to create the uniform dispersion of CNTs in a polymer matrix, as well as to increase the interfacial strength at the interfaces between CNTs and polymers.

Specifically, oxygenated defects, such as carbonyl, carboxylic acid, and hydroxyl groups, can be incorporated onto the surface of CNTs by oxidation of CNTs, which can occur, for example, by refluxing CNTs with concentrated acids. For example, Wagner and co-workers[29] reported the improved dispersion of SWNTs in poly(vinyl alcohol) (PVA) matrices and an increased tensile modulus by 79 % of SWNT/PVA nanocomposites relative to neat PVA by incorporating functional groups on the SWNT that can potentially hydrogen bond to PVA. They introduced oxygenated defects on SWNTs by mixing SWNTs with potassium hydroxide (KOH), and the functionalized SWNTs were characterized by UV-vis spectroscopy, which indicates in this study that the functionalization of the CNTs changes some of the sp^2 bonds of the pristine SWNTs into sp^3 bonds. The nanocomposites composed of functionalized SWNTs and PVA exhibited higher glass transition temperature (Tg) than neat PVA (68.8 ^{o}C → 74.3 ^{o}C), which suggests that potential hydrogen bonding between SWNTs and PVA exists and limited the molecular motions of PVA chains. Improved dispersion of nanocomposites was shown by optical microscopy. Their results suggest that functionalization can lead to uniform

dispersion of CNTs in a polymer matrix. In addition, the increased intermolecular interactions, probably hydrogen bonding in this work, between functionalized CNTs and polymers may result in improved interfacial strength, and thus increase the mechanical properties of final nanocomposites.

Similarly, Tong and co-workers[31] functionalized MWNTs by refluxing MWNTs with a mixture of sulfuric acid and nitric acid in order to induce oxygenated defects on MWNTs, and prepared nanocomposites of these oxidized MWNTs and the biopolymer chitosan. They reported the uniform dispersion of the MWNTs in chitosan, which was shown by optical microscopy, and an improvement of 93% in the tensile modulus of the chitosan/CNT nanocomposites relative to chitosan. This improvement is attributed to hydrogen bonding between the oxidized CNTs and the chitosan matrices. This result suggests that intermolecular hydrogen bonding between functionalized CNTs can result in better dispersion of CNTs and increased mechanical properties of polymer CNT nanocomposites.

In addition to the oxygenated defects on CNTs, Geng et al.[32] reported nanocomposites, which are composed of poly(ethylene oxide) (PEO) and fluorinated SWNTs (F-SWNTs) for potential intermolecular interactions between the functionalized SWNTs and PEO matrix. Upon the incorporation of 4 wt % F-SWNTs in the PEO matrix, the room temperature storage modulus of the nanocomposites increased by 400 % compared to pure PEO (0.3 GPa to 1.2 GPa). However, they indicated that mechanical properties of nanocomposites with pristine SWNTs were not improved with the same loading of the SWNTs. Their results suggest that chemical modification of CNTs can lead to the enhanced mechanical properties of nanocomposites with potential intermolecular

interactions.

1.2.3 Nanocomposite Preparation Processes

Several sample preparation processes, which include melt-mixing and solution casting, have been applied to polymer CNT nanocomposites as methods to create uniform and homogeneous dispersions of CNTs in polymer matrices. Experimental results show that the dispersion of CNTs, the interfacial strength between fillers and polymers, and consequently the mechanical properties of nanocomposites can be altered by varying the sample preparation method.

First, melt-mixing is a method to prepare nanocomposites by applying a shear field at high temperature to the polymer and CNT mixture.[19] Zhang et al.[30] prepared nanocomposites composed of polyamide 6 (PA6, nylon-6) and 1 wt % MWNTs, which were treated with nitric acid, by melt-mixing. They melt-mixed PA6 and MWNTs using a twin-screw mixer at 250 °C for 10 min with 100 rpm screw rotation speed. They reported the homogeneous dispersion of MWNTs in PA6 matrices, which was shown by imaging the fracture surfaces of the nanocomposite with scanning electron microscopy (SEM). Also, based on SEM images, the strong interfacial strength between MWNTs and PA6 was observed through the stretched and deformed MWNTs in the nanocomposite fracture surfaces. They reported the elastic modulus of nanocomposites with 1 wt % MWNTs and PA6 was higher by 115 % compared to that of neat PA6 (from 396.5 MPa to 852.4 MPa).

Similarly, Yang et al.[33] prepared nanocomposites, which were composed of atactic polypropylene (aPP) and MWNTs, by melt-mixing and analyzed the dynamic mechanical properties of the resultant nanocomposites. Specifically, they melt-mixed aPP

and MWNTs at 80 °C for 30 mins by using a Brabender mixer. They report that the storage modulus (E') of the nanocomposites improved as the weight fraction of MWNTs increased from 0 to 5 wt %. In addition, they showed the uniform dispersion of the MWNTs in an aPP matrix by fracture surface images from SEM. These results suggest that melt-mixing can be a useful method to improve the mechanical properties of MWNTs in a polymer matrix.

Solution-casting is also a nanocomposite preparation process that entails blending polymers and CNTs in solution, and obtaining the final nanocomposites by solvent evaporation or precipitation in a non-solvent.[19] Qian et al.[34] prepared solution-cast polystyrene(PS)/MWNT nanocomposites, and showed an increase of 36 – 42 % in the elastic modulus of the nanocomposites by adding 1 wt % MWNTs. They dissolved PS in toluene, and dispersed separately MWNTs in toluene by sonication. The polymer solution and MWNT suspension were then mixed together, and the final nanocomposites were recovered by evaporating the toluene. In addition to the improved mechanical properties, the uniform dispersion of MWNTs in a PS matrix was shown by TEM images of the nanocomposite films. Their work documents that a solution-casting process can be a facile and useful way for preparing polymer CNT nanocomposites.

Additionally, Du et al.[35] prepared nanocomposites composed of poly(methyl methacrylate) (PMMA) and SWNTs by blending PMMA and SWNTs in solution and precipitating in a non-solvent. They dissolved PMMA in dimethylformamide (DMF), and successively added the mixture of SWNTs and DMF, which was sonicated to improve the dispersion of the SWNTs in DMF. The mixture of PMMA and SWNTs in DMF were then precipitated in water. The homogeneous dispersion of SWNTs was observed by optical

microscopy. In addition, they presented results that showed elastic modulus of nanocomposites increased as the weight fraction of SWNTs increased from 0.5 to 2 wt %.

However, there still remain many challenges to creating a CNT-polymer nanocomposite with targeted dispersion for the optimal utilization of CNT in polymer nanocomposite. Furthermore, an investigation of the relationship between sample preparation processes and the dispersion of the CNTs, the intermolecular interactions between polymers and CNTs, and the final properties of nanocomposites has rarely been reported. In this study, the impact of the sample preparation process on the dispersion and properties of polymer MWNT nanocomposites is presented. Additionally, the impact of intermolecular interactions between the MWNT and polymer matrix on the mechanical properties of the polymer nanocomposites was also investigated. Nanocomposites, which are composed of 5 wt % MWNTs and poly(styrene-co-vinyl phenol) (PSVPh) random copolymers with 15 % of mole fraction of vinyl phenol groups, were prepared by three different sample preparation processes including melt-mixing and solution casting. The 15 % mole fraction of vinyl phenol groups of PSVPh was chosen from previous work in our lab.[36] Rasheed and coworkers[36] prepared nanocomposites composed of 5 wt % SWNTs or MWNTs and PSVPh with 0, 10, 20, 30, and 40 % mole fraction of vinyl phenol groups by solution casting. They analyzed the nanocomposites by IR to quantify the extent of intermolecular hydrogen bonding between the nanotubes and PSVPh, and measured tensile properties and electrical conductivity of the nanocomposites. In their work, it was shown that the optimum copolymer composition was 20 % vinyl phenol, in that this copolymer led to the formation of maximum intermolecular hydrogen bonding between the nanotubes and PSVPh, and optimal properties. In this study, we attempted to

synthesize 20 % vinyl phenol copolymers. However, the synthesis resulted in 15 % vinyl phenol copolymers, which were used in these experiments since we expect this to be sufficient to study the impact of intermolecular interactions on the properties of the nanocomposites. MWNTs were either oxidized to incorporate oxygenated defects or utilized as received. The mechanical properties of the resultant nanocomposites were characterized by dynamic mechanical analysis (DMA), and the extent of intermolecular hydrogen bonding between MWNTs and PSVPh matrices were quantified by infrared (IR) spectroscopy in order to correlate the extent of intermolecular interactions with the mechanical properties of nanocomposites and the importance of sample preparation technique on each of these molecular level parameters.

1.3 Sequestering Surface-modified Gold Nanoparticles in Diblock Copolymers: Starting Materials

Polymer based nanocomposites, which are composed of inorganic nanoparticles and block copolymers can be utilized in a variety of applications, such as photonic bandgap materials, optoelectronic materials, next-generation catalysts, and chemical sensors.[4,10,15] In order to obtain the required and tailored morphologies of the nanocomposites for these applications, the control and manipulation of sequestering nanoparticles in block copolymer matrices is needed.[10] Several theoretical and experimental studies to understand and observe the morphology of nanoparticle/block copolymer nanocomposites have been completed.

A theoretical understanding of the parameters that impact the morphology of nanoparticle/block copolymer nanocomposites was introduced by Balazs and co-

workers.[4] They report the simulation of the dispersion of spherical, hard nanoparticles into diblock copolymers by applying self-consistent field theory (SCFT) and density functional theory (DFT). To examine the importance of the affinity between the particles and polymer chains in specific domains of block copolymers, the Flory-Huggins interaction parameter, χ, which quantifies the enthalpic interaction between particles and polymers,[6] was incorporated into the simulation. For nanocomposites that include particle (P) and A-B diblock copolymers, the interaction parameter between the particles and the A chains, χ_{AP}, was set to zero by assuming particle surfaces are chemically identical to the A block of the diblock copolymers. In addition, the other interaction parameters, which are χ_{BP}, χ_{BA}, and χ_{AB}, were set to positive values, thus incorporating repulsive interactions between B chains and particles, and between B chains and A chains.

In this simulation, Balazs and co-workers show that the size and volume fractions of particles, as well as the characteristic of block copolymers impact the final morphology of the nanoparticle/block copolymer nanocomposites. Specifically, the size of the particles leads to different placement of the nanoparticle in the final nanocomposite. The large particles ($R = 0.3R_0$, R is the radius of a particle and R_0 is a root mean square end-to-end distance of the A block of the copolymer) self-assembled at the center of A domains. On the other hand, small particles ($R = 0.2R_0$) localize at the interface between the two blocks of the diblock copolymers. They explain that this result shows that the change in entropy of the polymer chains when the nanoparticle is introduced is the main factor that determines the final morphology of the diblock nanocomposites. Specifically, when large particles are used, the conformational entropy of the A chains is the main factor that determines the nanocomposite morphology. In contrast, when small particles

are used, the translational entropy of the A chains is dominant in determining the final nanocomposite morphology.

Additionally, Balazs and co-workers[37] generalized their results by including various interactions between particles and polymer chains: particles can interact with both A or B blocks in A-B-type diblock copolymer systems. In this simulation, they set χ_{AP} to be zero, but χ_{BP} varies from -1 to +1. The result of this simulation is that changing the various interactions between particles and polymers can impact the final nanocomposite morphologies. For example, for a nanocomposite that consists of large particles and diblock copolymers with 0.3 mole fraction A chains, a phase transition from the cylindrical phase to the lamellar morphology can occur with increasing χ_{BP} from -1 to +1. This study suggests that the final morphologies of nanocomposites can be impacted by varying the specific interactions between particles and polymers.

Several experimental efforts have been reported that sequester surface-modified inorganic nanoparticles in block copolymer systems. In most experimental cases, the enthalpic contributions between surface-modified particles (P) and polymer chains in one (A) of the blocks in diblock copolymers, χ_{AP}, is zero, i.e. neutral. Additionally, the enthalpic interaction between the particles and the other block (B) in A-B diblock copolymers, χ_{BP}, is usually positive, i.e. repulsive.

For example, Hashimoto and co-workers[11] reported sequestering surface-modified palladium (Pd) nanoparticles in a poly(2-vinly pyridine)-b-polyisoprene diblock copolymer (P2VP-b-PI), which microphase-separated into lamellar phases. The Pd nanoparticle surfaces were modified with poly(2-vinyl pyridine) (P2VP) homopolymers. In this work, P2VP-coated Pd nanoparticles were located at the center of the P2VP

lamellar domains in P2VP-b-PI diblock copolymers. This result suggests that sequestering the gold nanoparticles in the diblock copolymers results from the neutral interactions between the P2VP-coated Pd nanoparticles and the P2VP domain in the diblock copolymers, and the repulsive interactions between the P2VP-coated Pd nanoparticles and PI domains in the diblock copolymers.

Also, Thomas and co-workers[38] sequestered polystyrene (PS)-coated gold nanoparticles in poly(styrene-b-ethylenepropylene) diblock copolymers, which microphase-separated into lamellar phases. They reported that PS-coated nanoparticles were homogeneously dispersed in the PS domains in the diblock copolymers. In this work, repulsive interactions between the aromatic chain-coated gold nanoparticles and the aliphatic chains of the PEP block of the copolymer and neutral interactions between the PS-coated gold nanoparticles and the PS domains of the diblock copolymers control the placement of the nanocomposite in this system. As a result, the selective dispersion of nanoparticles in the diblock microphases was shown in this work.

Finally, Kramer and co-workers[39] reported sequestering either polystyrene (PS)-coated gold nanoparticles or gold nanoparticles coated with a 1:1 mixture of PS and poly(2-vinyl pyridine) (PVP) chains in poly(styrene-b-2-vinyl pyridine) (PS-b-P2VP) diblock copolymers, which microphase-separated into lamellar phases. In this work, PS-coated gold nanoparticles located at the center of the PS domains in the diblock copolymers. On the other hand, PS/PVP-coated gold nanoparticles were dispersed at the interface of PS lamellar domains and PVP lamellar domains in the diblock copolymers. These experimental results also show that nanoparticles can be sequestered in specific domains in diblock copolymers by controlling the repulsive and neutral interactions

between nanoparticles and polymers.

Little work, however, on diblock nanocomposites that incorporate attractive interactions between one of the blocks and the nanoparticles has been reported. Thus, in this study, the synthesis of starting materials to investigate a different approach for sequestering surface-modified gold nanoparticles in diblock copolymer systems is attempted. The long term goal is to investigate the diblock copolymer nanocomposites that incorporate enthalpic attractions between nanoparticles and polymer chains in one of the domains in diblock copolymers. That is, the system is designed such that χ_{AP} is negative by incorporating attractive hydrogen bonding between the gold nanoparticles and one of the blocks of the diblock copolymers.

Specifically, the synthesis of thiol-terminated poly(styrene-co-vinyl phenol) (PSVPh) random copolymers was attempted starting with bromine-terminated poly(styrene-co-4-tert-butoxystyrene) random copolymers by atom transfer radical polymerization (ATRP), followed by thiolation and hydrolysis. The thiol-terminated polymers can be utilized as a stabilizing ligand to synthesize PSVPh-coated gold nanoparticles in future work. The hydroxyl groups on gold nanoparticles can hydrogen bond with one block such as poly(2-vinyl pyridine) blocks of poly(styrene-b-2-vinyl pyridine) diblock copolymers. In addition, for this future study, gold nanoparticles, on which short-chain polystyrene (PS) were coated, were synthesized starting with bromine-terminated PS which was synthesized by ATRP, followed by thiolation.

CHAPTER 2

THE IMPACT OF SAMPLE PREPARATION ON POLYMER CARBON NANOTUBE NANOCOMPOSITES

2.1 Experimental

2.1.1 Synthesis of Poly(styrene-co-vinyl phenol) (PSVPh)

Poly(styrene-co-vinyl phenol) (PSVPh) random copolymers with 15% mole fraction of vinyl phenol groups were synthesized by synthesizing poly(styrene-co-acetoxystyrene) random copolymers via free radical polymerization followed by the hydrolysis of poly(styrene-co-acetoxystyrene) to poly(styrene-co-vinyl phenol). Styrene, 4-acetoxystyrene, 1,4-dioxane, 2,2'-azobisisobutyronitrile (AIBN), tetrahydrofuran (THF), and hydrazine hydrate were purchased from Aldrich, and utilized as received without further purification. The monomers, which were 255 ml of styrene and 45 ml of 4-acetoxystyene, were added to a 1000 ml three-neck, round-bottom flask, in which 0.126 g of 2,2'-azobisisobutyronitrile (AIBN) as an initiator were dissolved in 270 ml of anhydrous 1,4-dioxane, which was a solvent in this polymerization. All reactants were degassed by freeze-thaw processes repeated four times. The polymerization was conducted under nitrogen in an oil bath at 72 ^{o}C for 23 hrs. After polymerization, the resultant polymers were purified to remove unreacted monomers and solvent by dissolving in tetrahydrofuran (THF), precipitating in cold methanol, and drying under vacuum at 100 ^{o}C for 24 hrs. This purification process was repeated three times. The purified polymers were characterized by gel permeation chromatography (GPC) to measure molecular weight, and by nuclear magnetic resonance (NMR) to determine the

composition of the copolymer.

The hydrolysis of poly(styrene-co-acetoxystyrene) copolymers was completed to convert the acetoxy groups to hydroxyl groups. In a typical hydrolysis reaction, 40 g of poly(styrene-co-acetoxystyrene) was completely dissolved in 300 ml of dioxane, and then 120 ml of hydrazine hydrate was added into the polymer solution. This mixture was vigorously stirred under argon gas flow for 60 hrs at room temperature. After 60 hrs, the polymer was precipitated in cold methanol, filtered, and dried under vacuum at 120 ^{o}C for 38 hrs. The resultant polymers were characterized by GPC to determine molecular weight. NMR was utilized to verify the conversion of acetoxy groups to hydroxyl groups. Figure 2.1 shows the chemical equation to synthesize PSVPh copolymers.

2.1.2 Oxidation of Multi-walled Carbon Nanotubes and Raman Spectroscopy of MWNTs

The oxidation of multi-walled carbon nanotubes (MWNTs) was conducted to incorporate oxygenated defects onto multi-walled carbon nanotubes (MWNTs). In order to determine the optimum oxidation processes, four different oxidations, including 6M HNO_3, 3M HNO_3, $KMnO_4$, and RuO_4, were conducted, and as described in section 2.2.2, the best option which was the 6M HNO_3 treatment was chosen to oxidize the MWNTs to prepare polymer MWNT nanocomposites. MWNTs were purchased from Nanolab (Newton, MA, USA), and used as received without further purification processes. The outer diameters of the received MWNTs range from 10 to 20 nm, inner diameters from 5 to 9 nm, and lengths from 1 to 5 microns.[40]

For the 6M HNO_3 treatment,[41] 0.5 g MWNTs was refluxed in 100 ml of 6M

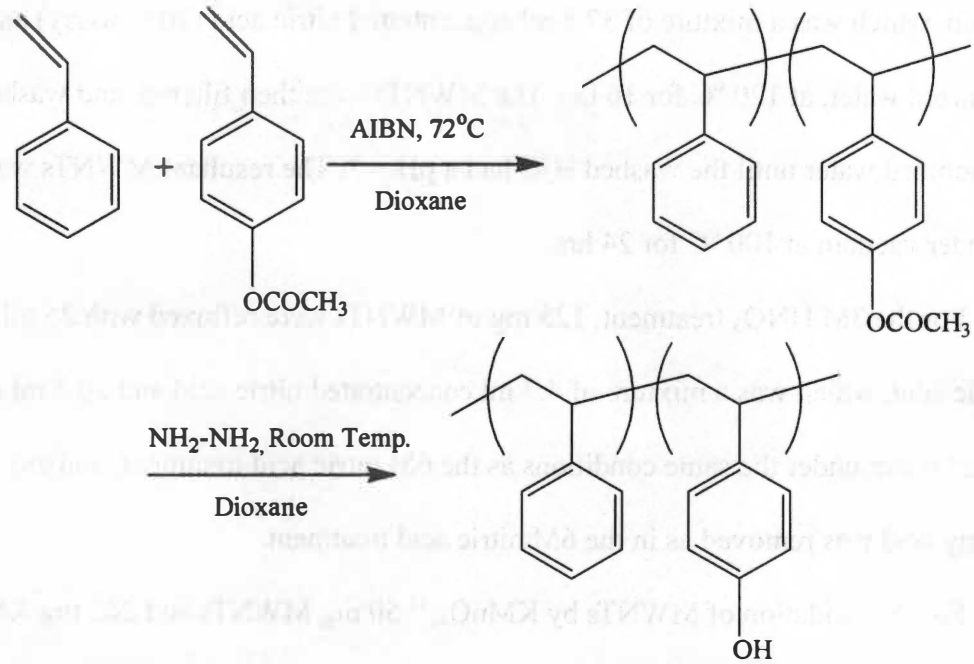

Figure 2.1 Scheme of synthesis procedure for PSVPh copolymers.

nitric acid, which was a mixture of 37.5 ml concentrated nitric acid (70 % assay) and 62.5 ml deionized water, at 120 °C for 16 hrs. The MWNTs were then filtered, and washed with deionized water until the washed H_2O had a pH ~ 7. The resultant MWNTs were dried under vacuum at 100 °C for 24 hrs.

For the 3M HNO_3 treatment, 125 mg of MWNTs were refluxed with 25 ml of 3M nitric acid, which was a mixture of 4.7 ml concentrated nitric acid and 20.3 ml of deionized water under the same conditions as the 6M nitric acid treatment, and any remaining acid was removed as in the 6M nitric acid treatment.

For the oxidation of MWNTs by $KMnO_4$,[41] 50 mg MWNTs and 262 mg $KMnO_4$ were mixed with 25 ml of 0.5M H_2SO_4, which was a mixture of 0.71 ml concentrated sulfuric acid (assay 95.4 %) and deionized water. This mixture was sonicated for 4 hrs at 40 - 45 °C. After sonication, the MWNTs were filtered, washed with concentrated HCl, followed by deionized water, 10mM NaOH (20 mg of NaOH dissolved in 50 ml water), deionized water, and 0.5M HCl (1.94 ml of conc. HCl with 48.06 ml water). The MWNTs were then washed with deionized water until the washed water had a pH ~ 7. The resultant MWNTs were dried under vacuum at 100 °C for 24 hrs.

Finally, for the RuO_4 treatment,[41] 1 mg of RuO_2 was mixed with 15 ml of sodium hypochlorite (NaOCl, 6wt %) to convert RuO_2 to RuO_4, which was verified by the appearance of the yellowish color of RuO_4.[41] Then, 50 mg of MWNTs was added, and mixed with the RuO_4 for three days at room temperature. The MWNTs oxidized or as received were characterized with Raman spectroscopy to quantify the efficiencies of the various oxidation procedures.

MWNTs with 6M nitric acid treatment was shown to be the most efficient

oxidation process among the 4 different oxidation procedures as described in section 2.2.2, was further purified with piranha solution to remove amorphous carbon, which is generated during the oxidation process.[41] In this process, 410 mg of MWNTs were mixed with 100 ml piranha solution (a mixture of H_2SO_4 and H_2O_2 in 4 to 1 volume ratio) and refluxed for 30 minutes at 70 °C. After piranha solution treatment, this mixture was diluted with deionized water, filtered, and washed with deionized water until the pH ~ 7. The final product was dried under vacuum at 100 °C for 24 hrs. These MWNTs, which were treated with 6M nitric acid and piranha solution, were utilized to prepare nanocomposites, and hereafter these MWNTs are called "oxidized MWNTs."

2.1.3 Preparation of Nanocomposites

Nanocomposites with oxidized MWNTs or unoxidized MWNTs were prepared with three different preparation procedures including melt-mixing and solution casting. Figure 2.2 illustrates the three nanocomposite preparation procedures used in this study.

The first method is a melt-mixing process, which is developed to mimic the process reported by Baskaran et al.[42] This method is denoted by "MM" in this study. In this process, 4.8 g of PSVPh copolymers were dissolved in 48 ml dimethylformamide (DMF). Either 0.24 g of oxidized or unoxidized MWNTs were separately sonicated using a Branson 2510 sonicator (Branson Ultrosonics Corporation, Danbury, CT, USA) in 240 ml DMF for 15 mins. The PSVPh polymer solution was added into this MWNT suspension in DMF, and sonicated for an additional 15 mins. This polymer/MWNT mixture in DMF was precipitated in cold methanol, filtered, and dried under vacuum at 120 °C for 30 hrs. These pre-nanocomposites were then melt-mixed using an Atlas

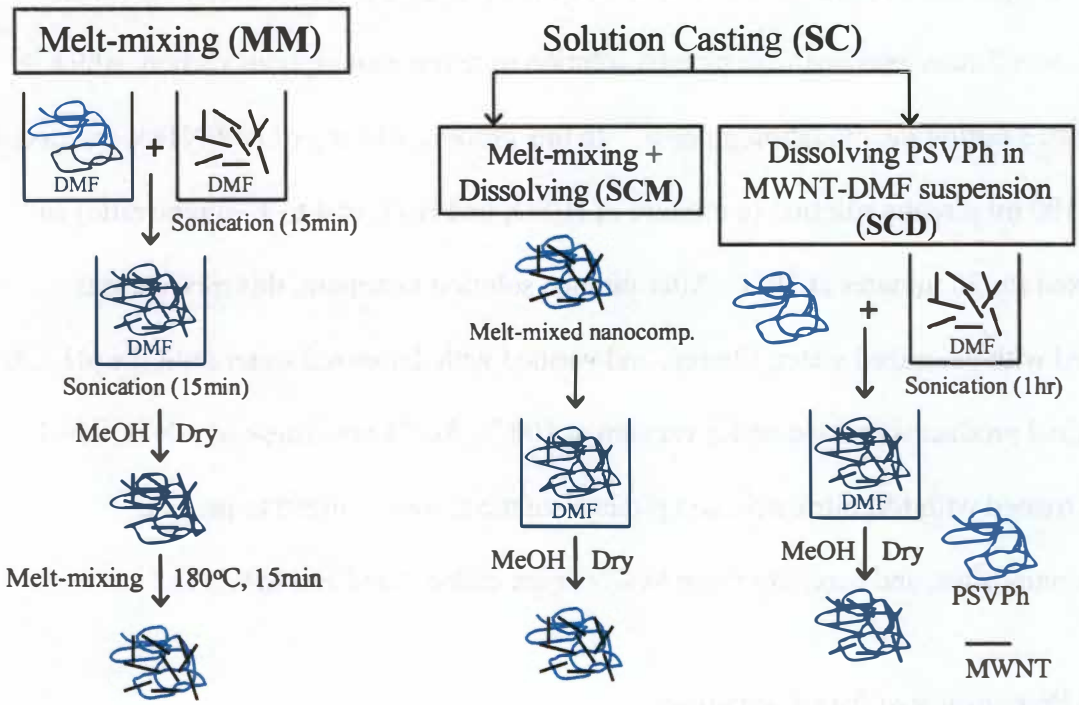

Figure 2.2 Scheme of sample preparation processes for polymer carbon nanotube nanocomposites. **MM**: Melt-Mixing process, **SCM**: Solution-Casting after Melt-mixing, and **SCD**: Solution-Casting after Dissolving polymers in MWNT-DMF suspension.

laboratory mixing molder (Atlas Electronic Devices, Chicago, USA) at 180 °C for 15mins with 60 rpm rotation speed. Hereinafter, the nanocomposites with oxidized MWNTs from this method are denoted by "MM_Oxidized," and nanocomposites with unoxidized MWNTs by "MM_Unoxidized."

Additionally, pure PSVPh copolymers without MWNTs were treated with the same procedures as the melt-mixed nanocomposites to precisely investigate the improvement of mechanical properties of the polymers with the incorporation of MWNTs. More specifically, 4.8 g of PSPVh copolymer was dissolved in 48 ml of DMF. 240 ml of DMF without MWNTs was separately sonicated for 15 min. Then the polymer solution was added into the DMF, which was sonicated, and then this solution was sonicated for additional 15 mins. The polymers were precipitated in cold methanol, filtered, and dried under vacuum at 120 °C for 30 hrs. Then this polymer was melt-mixed under the same conditions as the nanocomposite.

In addition to the melt-mixing process, two solution-casting methods were applied to prepare nanocomposites. The second method is a procedure that consists of melt-mixing, dissolving of the melt-mixed nanocomposites in DMF, and solution-casting. This procedure is denoted by "SCM," which refers to "solution casting after melt-mixing." In this procedure, 2.54 g of the melt-mixed nanocomposites from the MM method was completely dissolved in 181 ml of DMF (1.4 wt % of nanocomposites in DMF). Then, this mixture was precipitated in cold methanol. The final nanocomposite products were dried under vacuum at 120 °C for 30 hrs, and compression-molded for DMA as described in section 2.1.4. Nanocomposites with oxidized MWNTs from this method are denoted by "SCM_Oxidized," and nanocomposites with unoxidized MWNTs

by "SCM_Unoxidized." Melt-mixed PSVPh samples were also dissolved under the same conditions as the nanocomposite.

Finally, a third procedure, solution casting, was applied to prepare nanocomposites. This procedure is denoted by "SCD," which refers to solution-casting after dissolving polymers in DMF-MWNT suspension. In this procedure, 0.12 g MWNTs was separately sonicated in 180 ml DMF for 1 hr. Then, 2.4 g of PSVPh copolymers were added into this MWNT-DMF suspension, and completely dissolved. This polymer-MWNT solution was then precipitated in cold methanol and filtered. The final nanocomposite products were dried under vacuum at 120 °C for 30 hrs to remove any remaining solvent. Nanocomposites with oxidized MWNTs from this method are denoted by "SCD_Oxidized," and nanocomposites with unoxidized MWNTs by "SCD_Unoxidized." Additionally, PSVPh copolymers were treated with this procedure without MWNTs.

2.1.4 Dynamic Mechanical Analysis (DMA)

The mechanical properties of PSVPh and polymer carbon nanotube nanocomposites were analyzed by DMA (DMA Q800, TA instrument, New Castle, DE, USA) by applying a sinusoidal force with constant 1 Hz frequency from 25 °C to 145 °C for the PSVPh samples and 25 °C to 175 °C for the nanocomposite samples with a heating rate of 2 °C/min. The storage modulus (E'), loss modulus (E"), and tan(δ) were obtained by analyzing the relationship between the applied forces and the resultant strain.[32] The samples for DMA were prepared by compression-molding. Specifically, nanocomposite and PSVPh samples, which were cut into small pieces or ground into fine

powders, were loaded onto a rectangular template on a Carver laboratory hydraulic press (Fried S. Carver Inc., Monomonee Falls, WI, USA), and heated at 180 °C for 52 mins, which was regarded as enough time for nanocomposites or polymers to flow, and for possible porosity inside the samples to be removed. 2,500 psi pressure was then applied to the samples for 3 mins at 180 °C, and the template with the sample was slowly cooled under pressure until the temperature was around 50 °C. Then resultant rectangular samples, of which dimensions were 34.50 – 35.00 mm in length, 13.90 – 14.40 mm in width, and 1.2 – 1.3 mm in thickness, were separated from the template. The dimensions of each sample were carefully measured by calculating the average sizes of at least 10 spots of each sample, and this geometrical information was used to analyze the DMA data.

2.1.5 Infrared (IR) Spectroscopy

The intermolecular interactions between PSVPh and MWNTs were quantified by Fourier transform infrared spectroscopy (IR, Biored FTS-6000e). A PSVPh sample was scanned 1024 times with the range of 400 - 4000 cm^{-1} wavenumber at 4 cm^{-1} resolution. Spectroscopic information was corrected for KBr background information. Nanocomposite samples were characterized under the same condition as PSVPh sample analysis except for the number of scans, which were 25,000. Samples for IR were prepared by mixing 5 mg of pure copolymers or nanocomposites with 95 mg of potassium bromide (KBr), compressing this mixture into an IR pellet, and drying the compressed films under vacuum for 24 hrs at 100 °C.

2.1.6 Raman Spectroscopy and Scanning Electron Microscopy

MWNTs were characterized on Raman spectroscopy with a JY LabRam spectrometer using a CCD detector and He-Ne laser at 632.1 nm wavelength. The surface structures of MWNTs before and after oxidation were characterized using scanning electron microscopy (SEM, LEO 1525) with a 5 kV voltage using the in-lens detector as a secondary electron detector.

2.2 Results and Discussion

2.2.1 PSVPh Copolymer Characterization

GPC is widely used by polymer researchers to determine the molecular weight properties of polymers. The main principle of GPC is that the hydrodynamic volume of different polymer chains in a solvent are different, and elution time varies as polymer chains pass through porous columns.[43] With the elution time calibration of narrow molecular weight distribution polymers, the molecular weight of unknown polymers can be determined indirectly.[43] In this study, the molecular weight of poly(styrene-co-acetoxystyrene) and poly(styrene-co-vinyl phenol) copolymers were determined on a PL-GPC 120 (Polymer Laboratories Inc., Amherst, MA, USA) with two PLgel 5 micron mixed-B columns with the calibration of standard polystyrene with narrow molecular weight distribution in tetrahydrofuran (THF) as the elution solvent. Molecular weight of the poly(styrene-co-acetoxystyrene) copolymers was determined to have a number average molecular weight (Mn) of 114,000 g/mol, a weight average molecular weight (Mw) of 205,000 g/mol, and polydispersity (PDI) of 1.80. After hydrolysis, the molecular

weight of the poly(styrene-co-vinyl phenol) copolymers was found to have an Mn of 114,000 g/mol, Mw of 218,000 g/mol, and PDI of 1.91. The GPC data of polymers before and after hydrolysis shows that the hydrolysis reaction did not significantly impact the molecular weight of the polymers.

In polymer science, NMR spectroscopy is a useful tool to characterize the structure of polymers by characterizing the chemical environment of its protons.[44] In this work, NMR was utilized to determine the chemical composition of the random copolymers. Specifically, NMR was utilized to determine the mole fraction of acetoxy groups in the synthesized poly(styrene-co-acetoxystyrene) copolymers and as a tool to verify the conversion of acetoxy groups to hydroxyl groups. Figure 2.3 (a) shows the ^{1}H spectrum of poly(styrene-co-acetoxystyrene) copolymers dissolved in deuterated chloroform. The mole fraction of acetoxy groups was calculated based on the number of protons of each type present. The integration of proton groups provides information on the mole fraction of each functional group. In this analysis, the mole fraction of styrene groups is set to x, and number of acetoxy groups is y. Based on the presence of 5 aromatic protons in each styrene group and 4 aromatic protons in each acetoxystyrene group, the following equation is formed: $5x + 4y = 10.67$, where 10.67 is the area of the aromatic (6.2 – 7.2 ppm) peaks in the NMR curve. In addition, the integration of the 3 methyl protons in the acetoxy groups, which occurs around 2.3 ppm, provides the following equation: $3y = 1$. From these two equations, $x = 1.86$ and $y = 0.33$. Therefore, the fraction of acetoxy groups is 15.1 % based on the following fact that the % of acetoxy groups = $[y/(x+y)]*100$. Figure 2.3 (b) shows the ^{1}H spectrum of poly(styrene-co-vinyl phenol) copolymers after the hydrolysis of poly(styrene-co-acetoxystyrene) copolymers. As can

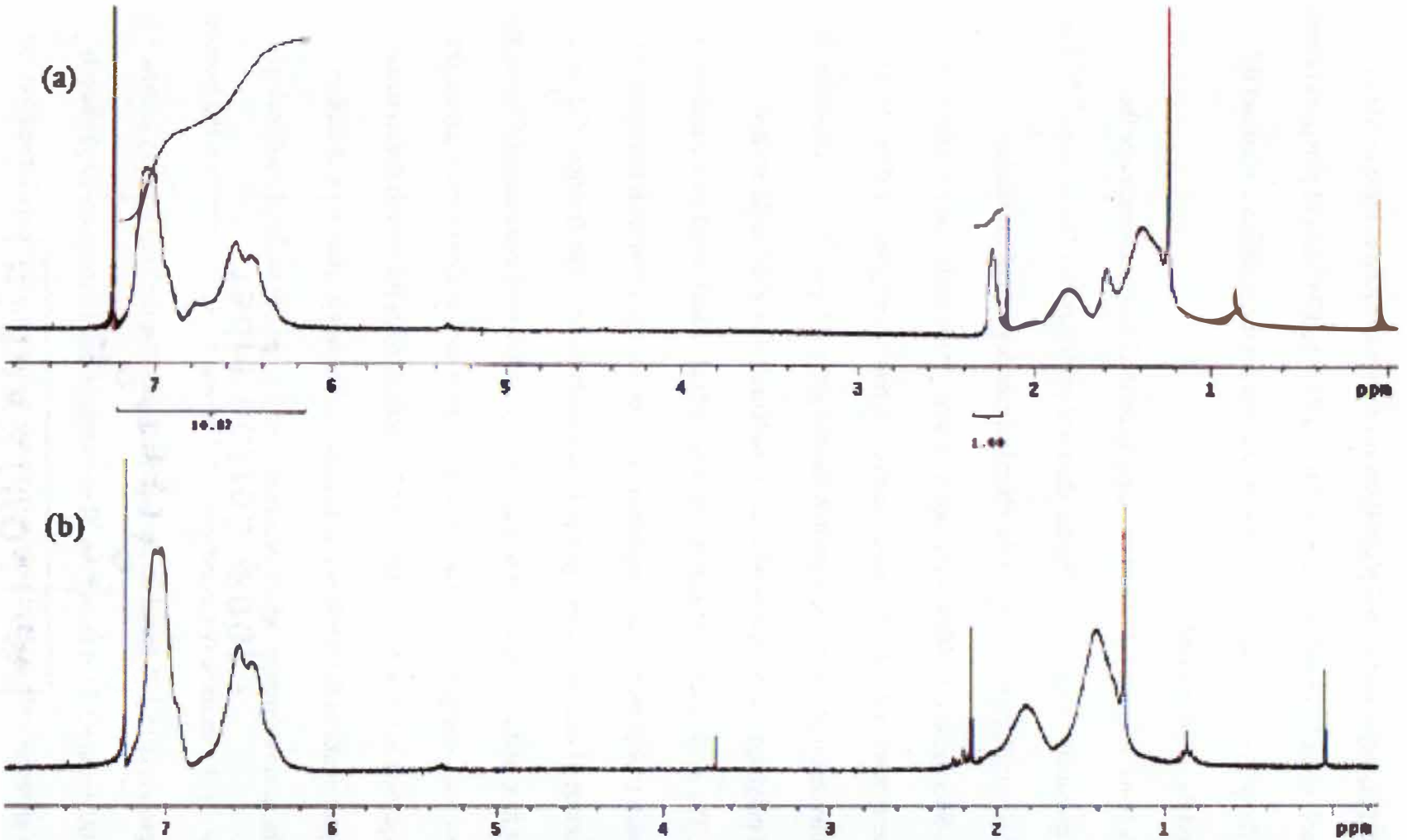

Figure 2.3 ^{1}H spectra of (a) poly(styrene-co-acetoxystyrene) copolymers and (b) poly(styrene-co-vinyl phenol) copolymers after hydrolysis.

be seen in Figure 2.3 (b), the acetoxy proton peaks around 2.3 ppm disappears, which indicates the conversion of the acetoxy groups to hydroxyl groups.

2.2.2 Characterization of MWNTs

Raman spectroscopy has been widely utilized to characterize functionalized defects of CNTs, and to investigate interactions between CNTs and polymers.[29,45] In general, CNTs shows the following representative features of Raman spectroscopy: the disorder-induced D band (~ 1290 - 1320 cm^{-1}), the tangential mode G band (~ 1560 - 1600 cm^{-1}), and the second-order overtone D* of the D band (~ 2560 - 2610 cm^{-1}).[29] Among these bands, the D band indicates disorder in the structure of the CNTs, which can be used to quantify the amount of defects in CNTs. In addition, the G band indicates the graphite structure in CNTs, which can be used to quantify the amount of pristine structures in CNTs.[28,45] Thus, the ratio of the intensity of the D band [I(D)] to the intensity of the G band [I(G)] provides a method to quantify the amount of defects in CNTs.[41] In this study, the numerical values of I(D)/I(G) from the Raman spectrum of the MWNTs were used to quantify the amount of oxygenated defects of the MWNTs for the 4 different oxidation processes. The optimum oxidation process, which was 6M HNO_3 oxidation, was chosen for the nanocomposite systems that maximized the oxygenated defects on MWNTs.

Figure 2.4 shows the Raman spectra of the oxidized MWNTs and unoxidized MWNTs, and this data is summarized in Table 2.1. As can be seen in the figure and table, 6M nitric acid treatment was the most efficient oxidation process among the 4 oxidation methods in that the highest value of I(D)/I(G), suggesting that the 6M nitric acid

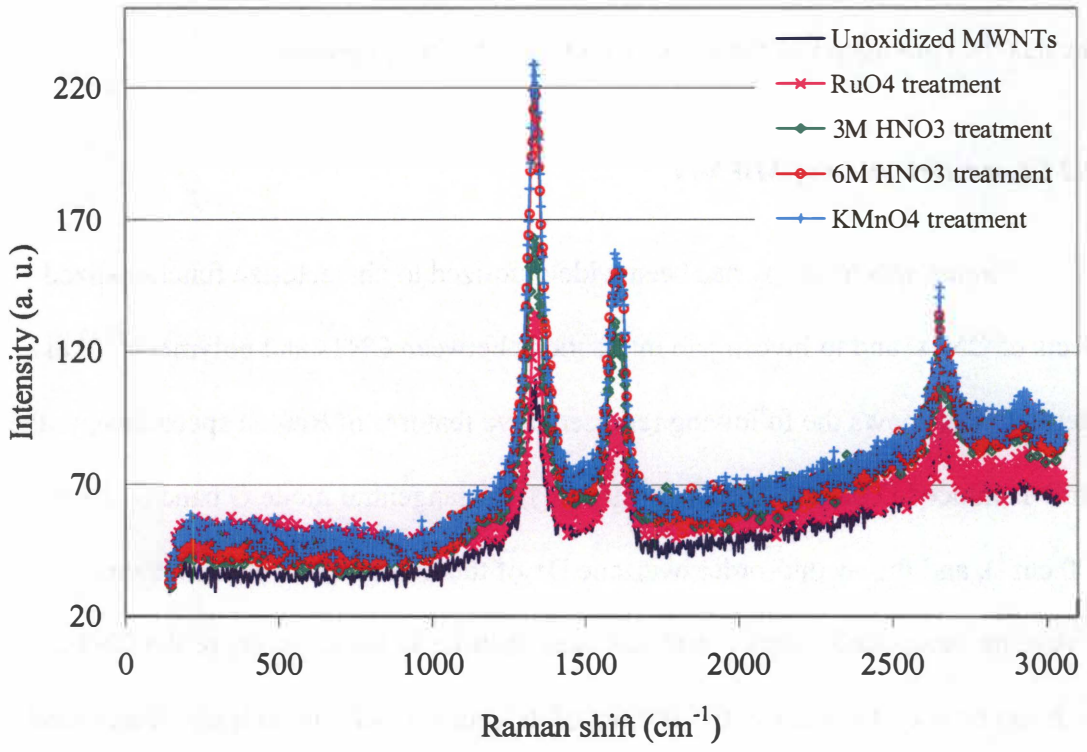

Figure 2.4 Raman spectra of oxidized MWNTs from 4 different oxidation processes and unoxidized MWNTs.

Table 2.1 Summary of Raman spectroscopy of MWNTs treated with various oxidizing agents or untreated MWNTs.

	I(D)	D band peak	I(G)	G band peak	I(D)/I(G)
6M HNO_3	219.35	1335	147.75	1610	1.49
3M HNO_3	163	1332	131	1598	1.24
$KMnO_4$	228.75	1332	157.25	1598	1.46
RuO_4	133.75	1335	92.25	1592	1.45
Unoxidized MWNTs	109.5	1338	92.75	1598	1.18

generates more oxygenated defects in MWNTs than other oxidizing agents, and thus the defects can provide more sites for potential hydrogen bonding with a PSVPh matrix. Additionally, MWNTs with 6M nitric acid treatment were further purified with piranha solution to remove amorphous carbon, which may be generated during oxidation. Figure 2.5 shows SEM images of MWNTs (a) without oxidation, (b) with 6M nitric acid treatment, and (c) 6M nitric acid and piranha solution treatment. As can be seen in the images, the oxidation process and piranha solution treatment does not significantly impact the overall structure of the MWNTs.

2.2.3 Dynamic Mechanical Analysis

Dynamic mechanical analysis (DMA) is a useful tool to investigate the molecular relaxation of polymer chains. Polymeric materials are viscoelastic, which means that they have both elastic and viscous response to applied forces.[1] Elastic behavior is related to the energy stored in an elastic solid, and the viscous behavior is related to the energy dissipation of a viscous liquid.[1] The storage and loss modulus can be defined by applying a periodic loading as:[1]

$$\varepsilon = \varepsilon_0 \sin(\omega t) \tag{2.1}$$

where ω is the frequency of the applied strain, ε_0 is the strain amplitude, and t is time. The stress required in a viscoelastic material to realize this sinusoidal strain can be expressed as the following form:

$$\sigma = \sigma_0 \sin(\omega t + \delta) \tag{2.2}$$

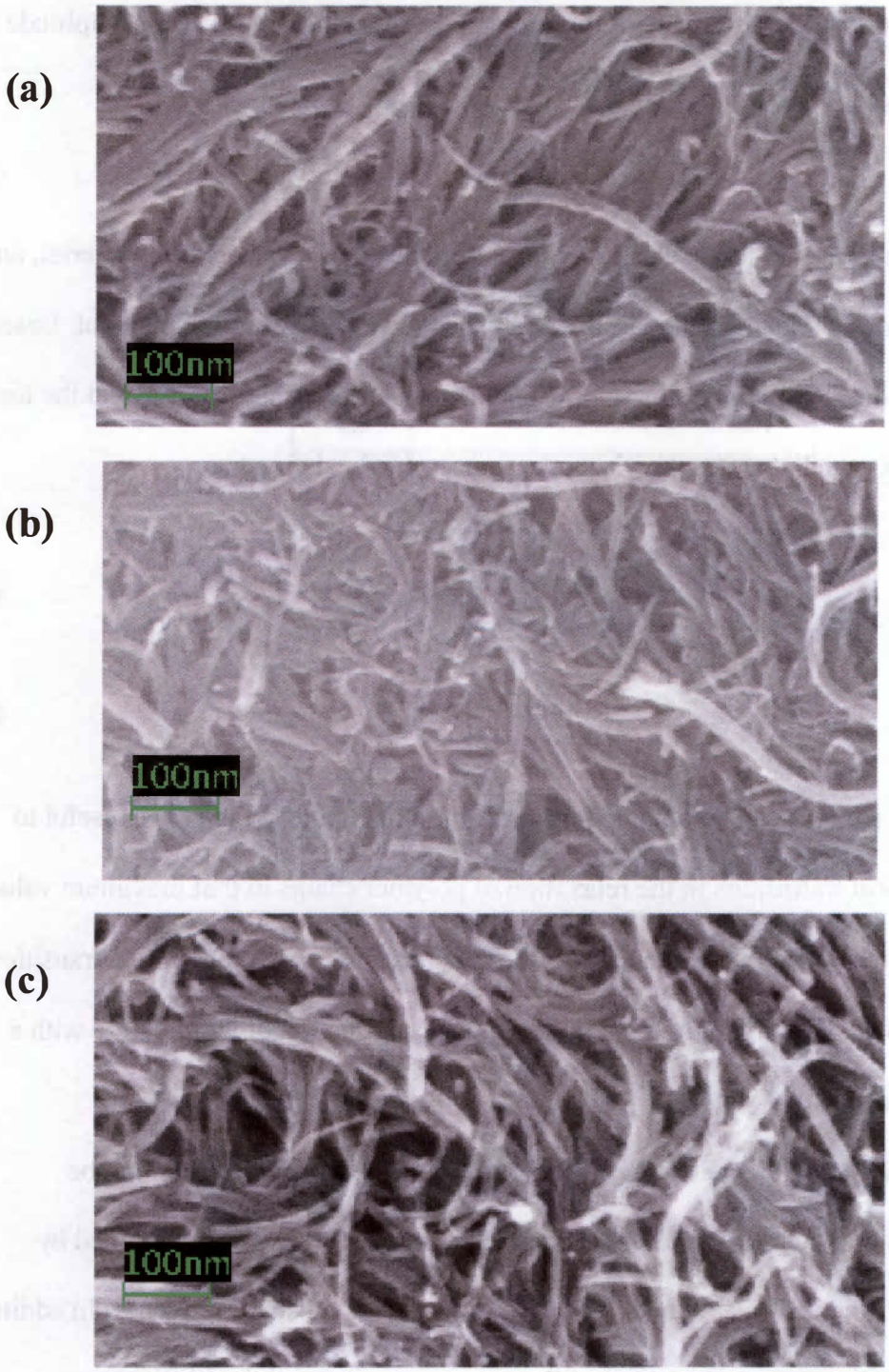

Figure 2.5 Representative SEM images of MWNTs. (a) unoxidized, (b) 6M nitric acid treated, and (c) 6M nitric acid and then piranha solution treated MWNTs.

where δ is the phase difference of the strain and stress, and σ_0 is stress amplitude. This equation can be rewritten as:

$$\sigma = \sigma_0 \cos\delta \sin\omega t + \sigma_0 \sin\delta \cos\omega t \tag{2.3}$$

The first term is related to the elastic response (in-phase) of a viscoelastic material, and the second term is related to the viscous response (out-of-phase) of the material. Based on this concept, the storage modulus (E'), which denotes the elastic response, and the loss modulus (E"), which denotes the viscous response, can be defined as:

$$E' = \frac{\sigma_0 \cos\delta}{\varepsilon_0} \tag{2.4}$$

$$E'' = \frac{\sigma_0 \sin\delta}{\varepsilon_0} \tag{2.5}$$

Additionally, tan (δ) can be obtained from the ratio of E' to E". Tan (δ) is useful to investigate local transitions in the relaxation of polymer chains in that maximum values of tan (δ) can be observed when a transition, such as glass transition or beta transition, occurs. In DMA, E' and E" are often investigated as a function of temperature with a constant frequency.

In this study, the mechanical properties of the polymer carbon nanotube nanocomposites from different sample preparation procedures were determined by investigating E' and E" as a function of temperature with constant frequency. In addition, the glass transition temperature (Tg) of the nanocomposites and the PSPVh were determined by analyzing the peaks of the tan (δ) curves. The E' of each nanocomposite was normalized by the E' of the PSVPh matrix, prepared by identical preparation

procedures, and this data is plotted as a function of (T – Tg). T is the temperature of the storage modulus measurement, and Tg is the glass transition temperature of each sample, which was obtained from a tan (δ) peak. In this study, the nanocomposites have Tg in the range of 126 to 130 °C. Figure 2.6 shows the E' of the PSVPh, prepared by MM, SCM, or SCD. As can be seen, the PSVPh copolymers have E' near 2800 MPa at 27 °C.

Figure 2.7 shows the ratio of E'[nanocomposites] to E'[PSVPh] as a function of (T – Tg) of the MM nanocomposites with oxidized or unoxidized MWNTs. As can be seen in Figure 2.7, this normalized storage modulus was higher than 1 at all temperatures, which suggests that the nanocomposites are more rigid than PSVPh, and thus the mechanical properties of nanocomposites are improved relative to that of the pure PSVPh. Additionally, the E' of the nanocomposites with oxidized MWNTs is higher than that of the nanocomposites with unoxidized MWNTs at all temperatures.

The mechanical properties of the nanocomposites can be impacted by the final morphologies of the MWNT nanocomposites, which are formed during the sample preparation processes in that the uniform dispersion of CNTs is required to realize the improvement of the ultimate properties of the nanocomposites. The morphologies of nanocomposites can be impacted by the formation of intermolecular interactions between polymers and MWNTs, which can also be impacted by the sample preparation processes. One way to interpret the DMA data in Figure 2.7 is that it is possible that the MWNTs can be "wrapped"[42] by polymer chains during melt-mixing under a high shear field at high temperature. This wrapping process can result in a nanocomposite morphology that is very stable. That is, melt-mixing may provide enough time for the formation of a steady state morphology in the final nanocomposites. Furthermore, the higher E' ratio of

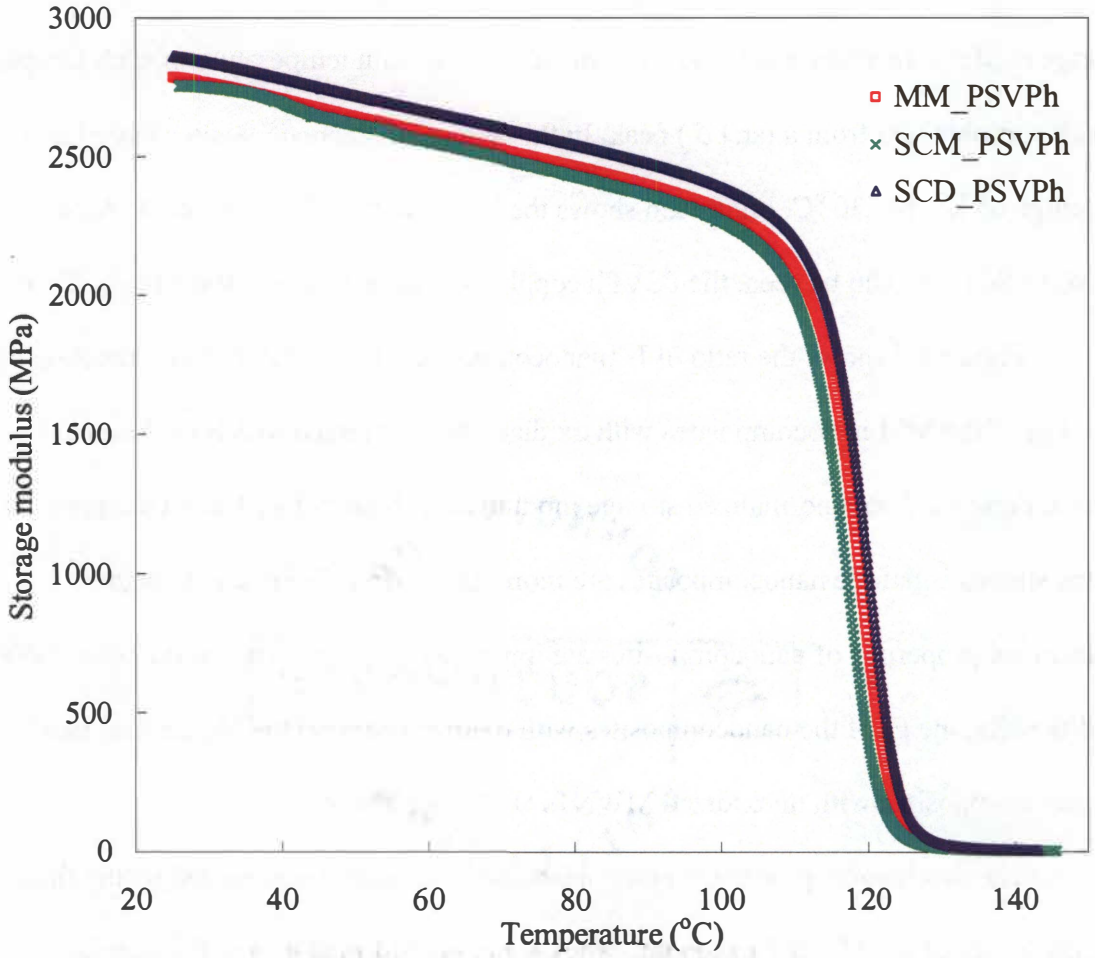

Figure 2.6 Storage modulus of PSVPh samples prepared from MM (MM_PSVPh), SCM (SCM_PSVPh), or SCD (SCD_PSVPh) methods as a function of temperature.

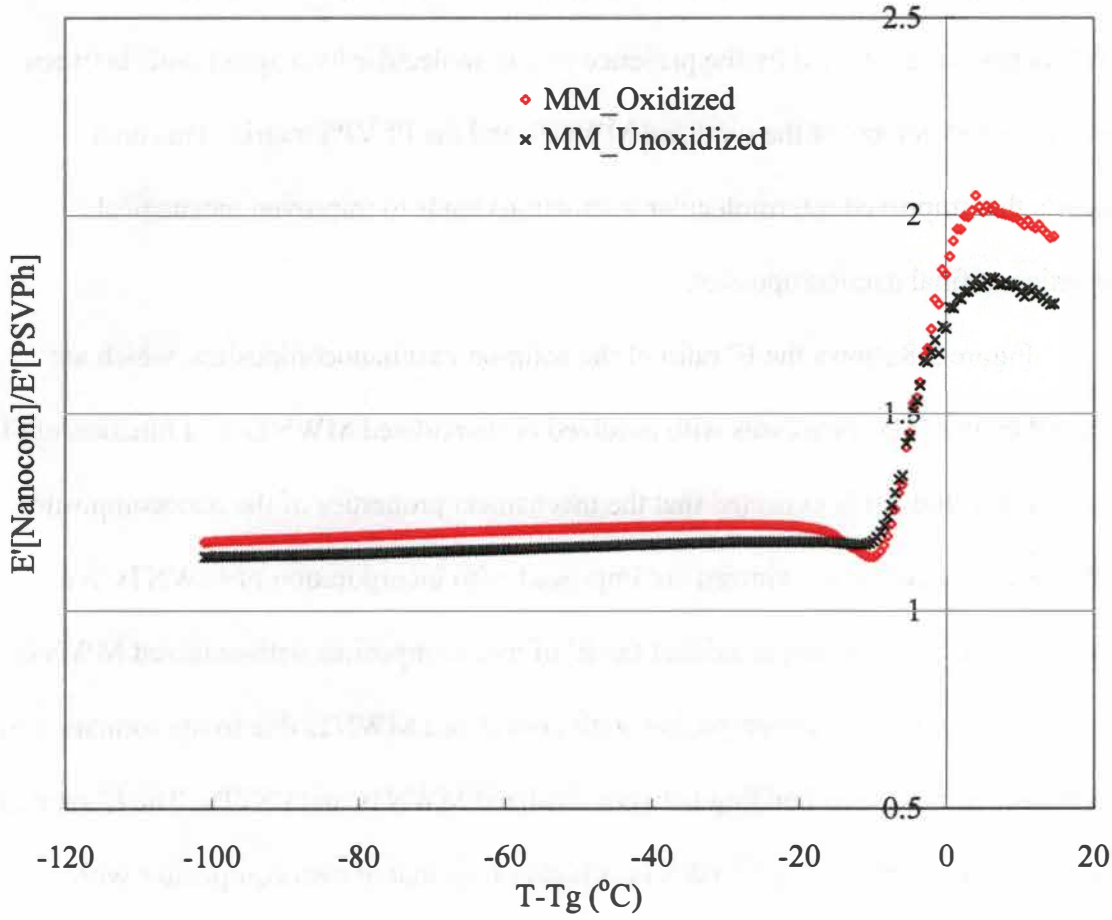

Figure 2.7 Storage modulus ratio of MM nanocomposites with oxidized (◊) and unoxidized (x) MWNTs normalized to that of the PSVPh as a function of temperature (T – Tg).

nanocomposites with oxidized MWNTs than that of nanocomposites with unoxidized MWNTs may be explained by the presence of intermolecular hydrogen bonds between the oxygenated defects of the oxidized MWNTs and the PSVPh matrix. This data suggests that improved intermolecular interactions leads to improved mechanical properties of final nanocomposites.

Figure 2.8 shows the E' ratio of the solution-cast nanocomposites, which are prepared by the SCM processes with oxidized or unoxidized MWNTs as a function of (T – Tg). In this study, it is expected that the mechanical properties of the nanocomposites with either oxidized or unoxidized are improved with incorporation of MWNTs in a PSVPh matrix. It is also expected that the E' of nanocomposites with oxidized MWNTs are higher than that of nanocomposites with unoxidized MWNTs due to the formation of intermolecular hydrogen bonding between oxidized MWNTs and PSVPh, The E' ratio of nanocomposites with oxidized MWNTs is higher than that of nanocomposites with unoxidized MWNTs below Tg, but lower than those realized by the MM method. However, nanocomposites with unoxidized MWNTs exhibit unexpectedly higher E' ratio than nanocomposites with oxidized MWNTs above Tg. These mechanical properties of SCM samples can be explained by the presence of morphology that is different in the MM samples, which will impact the mechanical properties of the final nanocomposites. Specifically, by dissolving the MM nanocomposites in DMF and quenching it in methanol, the MM samples may lose the "wrapped" morphology. The precipitation may not provide sufficient time for the final SCM nanocomposites to reach a stable morphology. Therefore, the DMA data of the SCM nanocomposites suggests that the loss of the wrapping morphologies in SCM nanocomposites may lead to poor mechanical

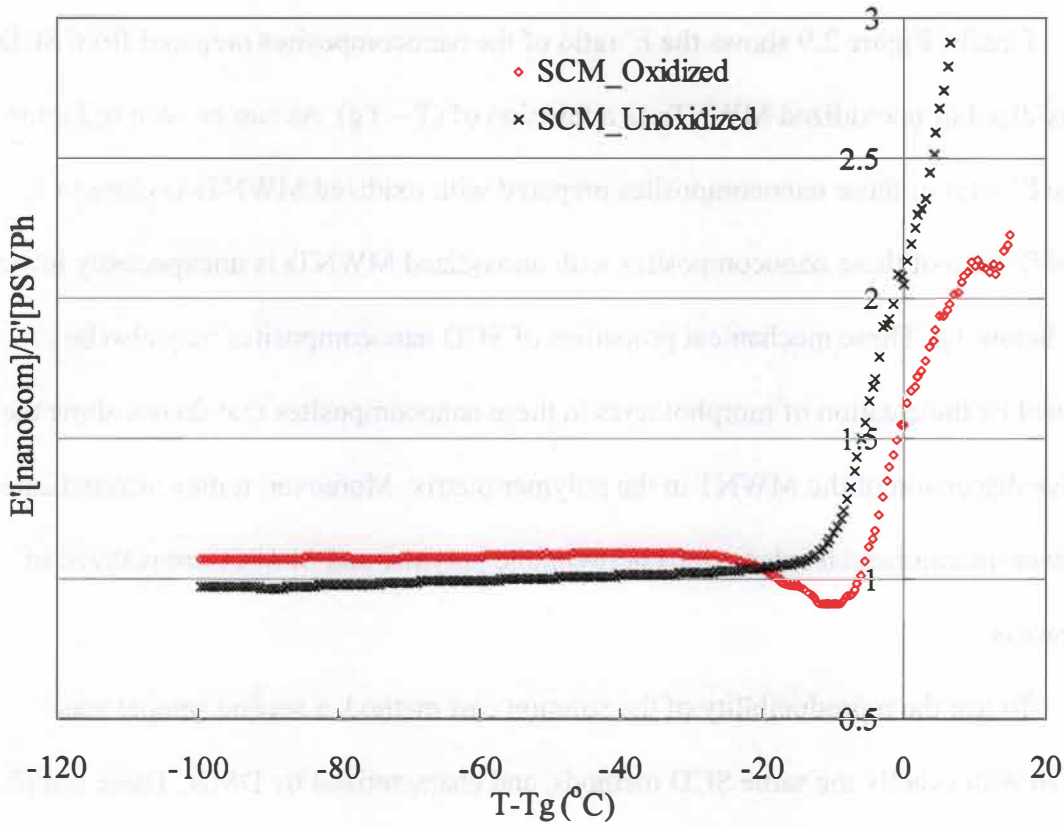

Figure 2.8 Storage modulus ratio of SCM nanocomposites with oxidized and unoxidized MWNTs normalized to that of the PSVPh as a function of temperature (T – Tg)

properties of the final SCM nanocomposites.

Finally, Figure 2.9 shows the E' ratio of the nanocomposites prepared from SCD with oxidized or unoxidized MWNTs as a function of (T – Tg). As can be seen in Figure 2.9, the E' ratio of these nanocomposites prepared with oxidized MWNTs is close to 1, and the E' ratio of these nanocomposites with unoxidized MWNTs is unexpectedly lower than 1 below Tg. These mechanical properties of SCD nanocomposites may also be explained by the creation of morphologies in these nanocomposites that do not allow the effective dispersion of the MWNT in the polymer matrix. Moreover, it may also indicate that fewer intermolecular interactions between the polymer and MWNT are realized in this process.

To test the reproducibility of the solution cast method, a second sample was prepared with exactly the same SCD methods, and characterized by DMA. These samples are denoted by "SCD_2nd." Furthermore, these SCD_2nd samples were further exposed to melt-mixing, and also characterized by DMA. These samples were denoted by "SCD&MM." Figure 2.10 shows the E' ratio of the second nanocomposite sample created by the SCD procedure. The E' ratio of this nanocomposite with oxidized MWNTs is close to that of the nanocomposite with unoxidized MWNTs at low temperatures (Tg – 70 < T < Tg – 30). At higher temperature, the E' ratio of the nanocomposites with oxidized MWNTs is higher than that of the nanocomposites with unoxidized MWNTs. This DMA data differs from that in Figure 2.9 although nanocomposites were prepared from the same SCD procedure. This can be explained as resulting from the non-equilibrium state of final nanocomposite morphology that results from this sample preparation procedure. That is, the DMA data of SCD and SCD_2nd samples suggest that

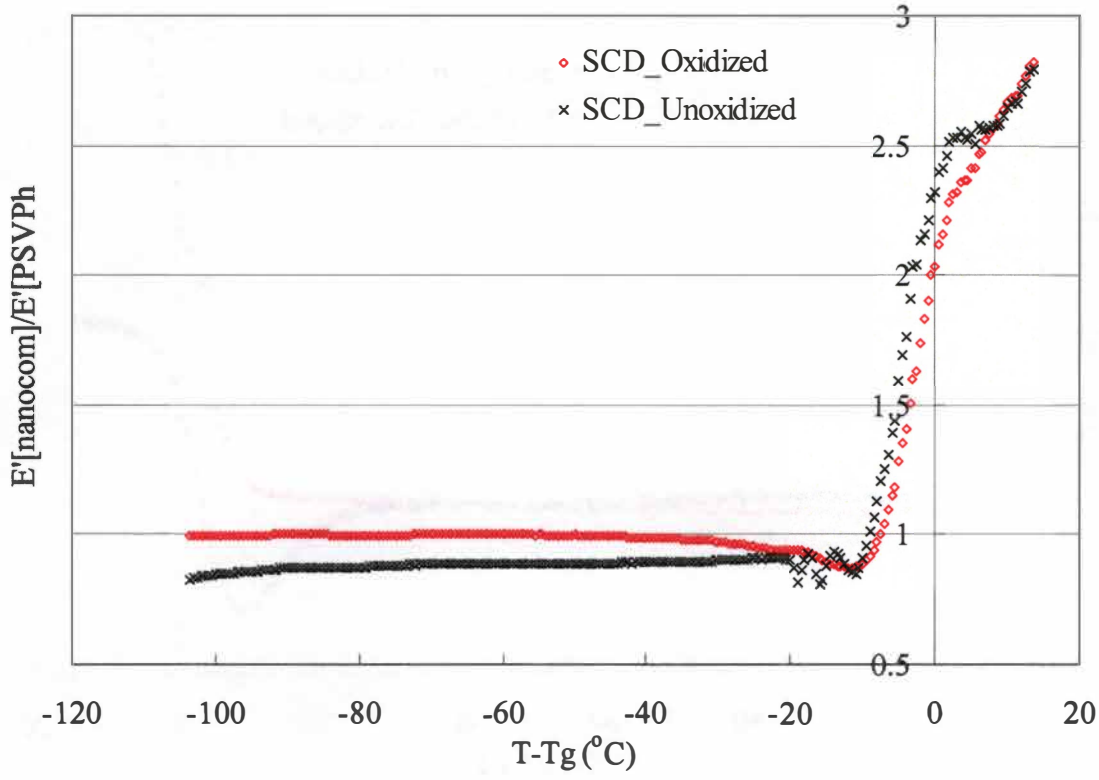

Figure 2.9 Storage modulus ratio of SCD nanocomposites with oxidized and unoxidized MWNTs normalized to that of the PSVPh as a function of temperature (T – Tg).

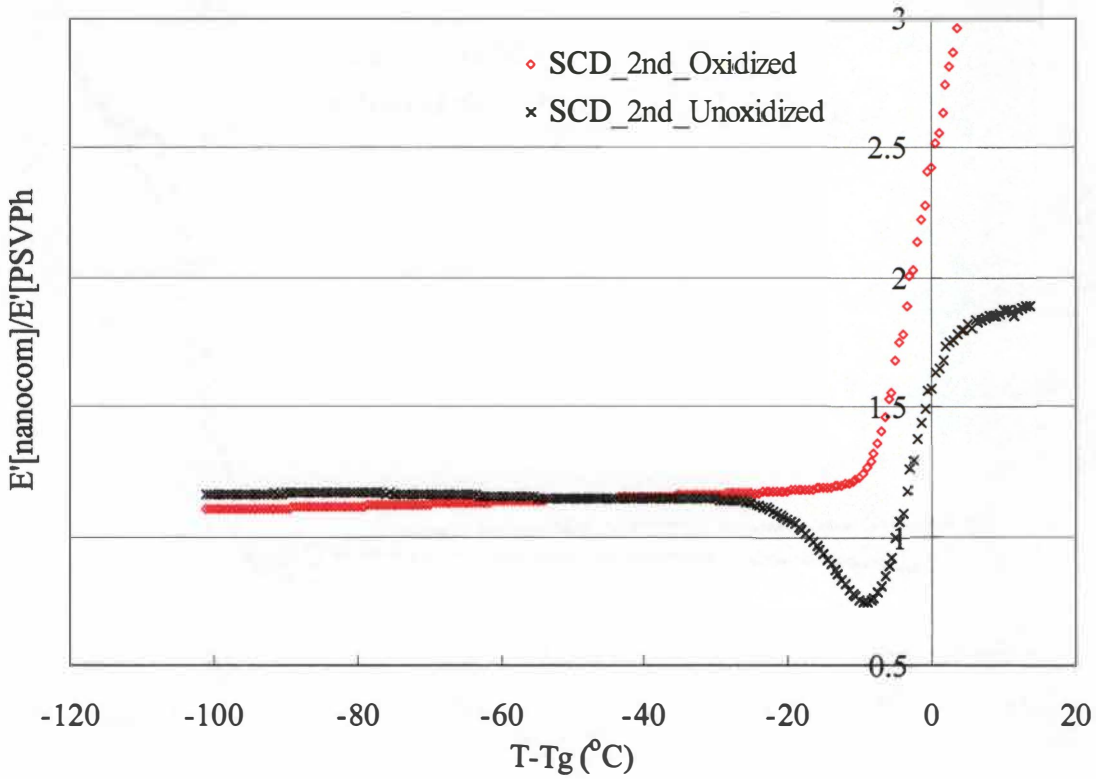

Figure 2.10 Storage modulus ratio of SCD_2nd samples with oxidized or unoxidized MWNTs to that of PSVPh as a function of temperature (T – Tg).

the system attains non-equilibrium morphology, which results from the rapid quenching of the MWNT/PSVPh/DMF solution in methanol, and can lead to the variation of mechanical properties of final nanocomposites.

Lastly, Figure 2.11 shows the E' ratio of the nanocomposites prepared from SCD and followed melt-mixing process. As can be seen in Figure 2.11, the E' ratio of this nanocomposite with oxidized MWNTs is higher than that of nanocomposite with unoxidized MWNTs. The E' ratio of the nanocomposite with oxidized MWNTs is greater than 1, and the E' ratio of the nanocomposite with unoxidized MWNTs is close to 1 at low temperatures. When the DMA data of SCD&MM samples in Figure 2.11 is compared with that of SCD_2nd samples in Figure 2.10, the E' ratio of the solution-cast nanocomposites with oxidized MWNTs increases after melt-mixing. At high temperature, E' ratios of oxidized or unoxidized MWNTs are similar. Additionally, these mechanical properties of nanocomposites from SCD&MM in Figure 2.11 appear similar with those of the nanocomposites from MM shown in Figure 2.7.

The DMA data of these SCD&MM samples can be explained by the presence of a steady state morphology in the final nanocomposites, which may be formed during melt-mixing. Specifically, the DMA data suggests that melt-mixing may provide enough time to form stable morphologies of final nanocomposites by the formation of intermolecular interactions during mixing. Evidence of these stable morphologies is best given by the similarity of the DMA results of the SCD&MM samples in Figure 2.11 and the MM samples in Figure 2.7. Additionally, the DMA data of the SCD&MM samples suggests that the melt-mixing process provides more reproducible samples than the solution casting method. That is, melt-mixing may provide sufficient time to form

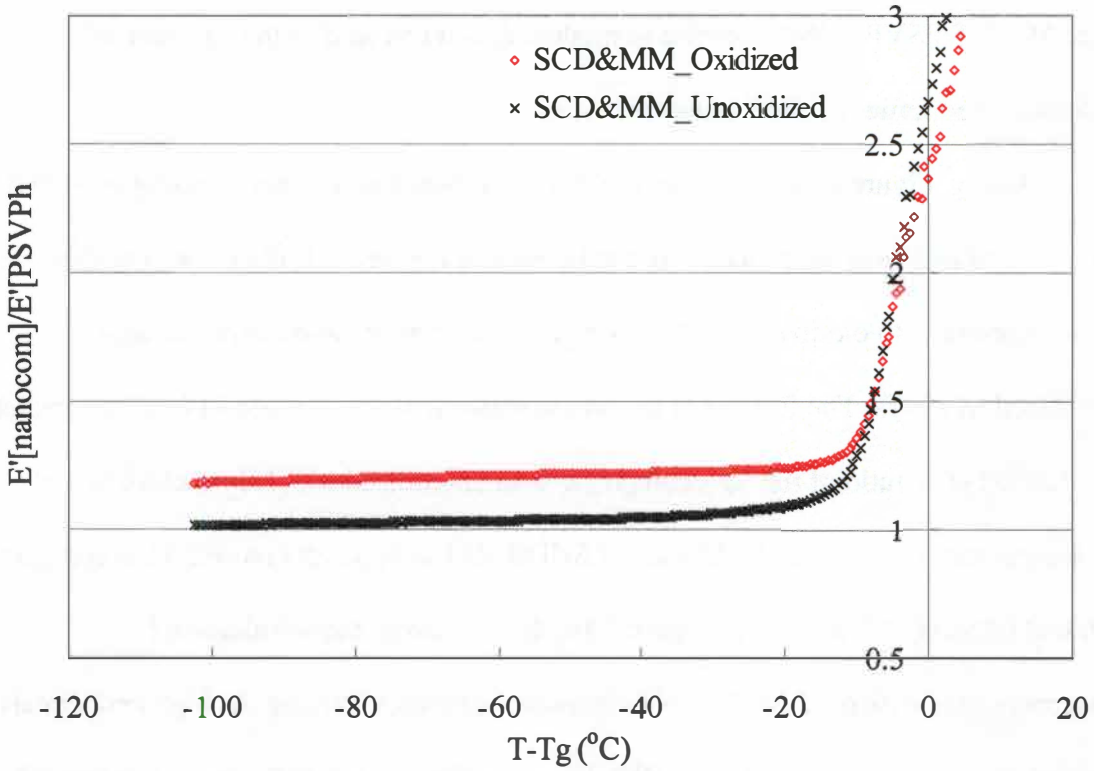

Figure 2.11 Storage modulus ratio of SCD&MM samples with oxidized or unoxidized MWNTs to that of PSVPh as a function of temperature (T – Tg).

intermolecular hydrogen bonding between MWNTs and a PSVPh matrix than solution casting.

Finally, Figure 2.12 and 2.13 show the E' ratio of the nanocomposites, which were prepared from the three different sample preparation procedures (MM, SCM, and SCD), with oxidized and unoxidized MWNTs respectively. At low temperature (Tg – 100 < T < Tg – 10), the nanocomposites from melt-mixing (MM) with either oxidized or unoxidized MWNTs shows a higher E' ratio than those from solution casting (SCM and SCD). This indicates that melt-mixing leads to more improvement in the mechanical properties of the final nanocomposites when compared to solution casting. Additionally, the highest E' ratio was shown in a melt-mixed nanocomposite with oxidized MWNTs. This improvement of mechanical properties may contribute to the steady state of the melt-mixed nanocomposite morphologies, and provide a higher probability to incorporate intermolecular interactions between the MWNTs and the PSVPh matrix than in solution casting.

2.2.4 Infrared Spectroscopy of Nanocomposites: Correlate Mechanical Properties with Intermolecular Interactions

Infrared (IR) spectroscopy is a useful method to identify specific functional groups of polymers since certain molecular motions absorb specific wavelengths of radiation. That is, in the absorption process of IR spectroscopy, when the frequencies of infrared radiation correspond to the natural vibrational frequencies of a molecule, the frequencies of IR radiation are absorbed in bonds of a molecule.[44] In this study, the hydroxyl group (O–H) stretching vibration at 3100 – 3700 cm^{-1} was analyzed for

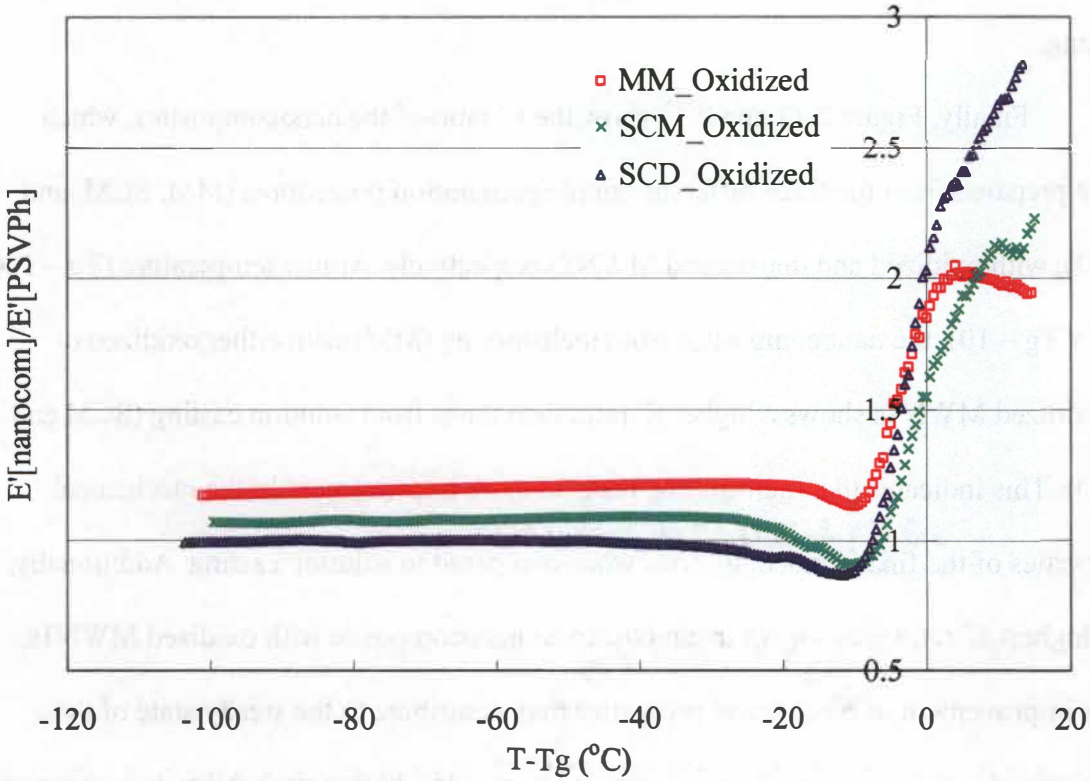

Figure 2.12 Summary of storage modulus ratio of nanocomposites with oxidized MWNTs from MM, SCM, or SCD.

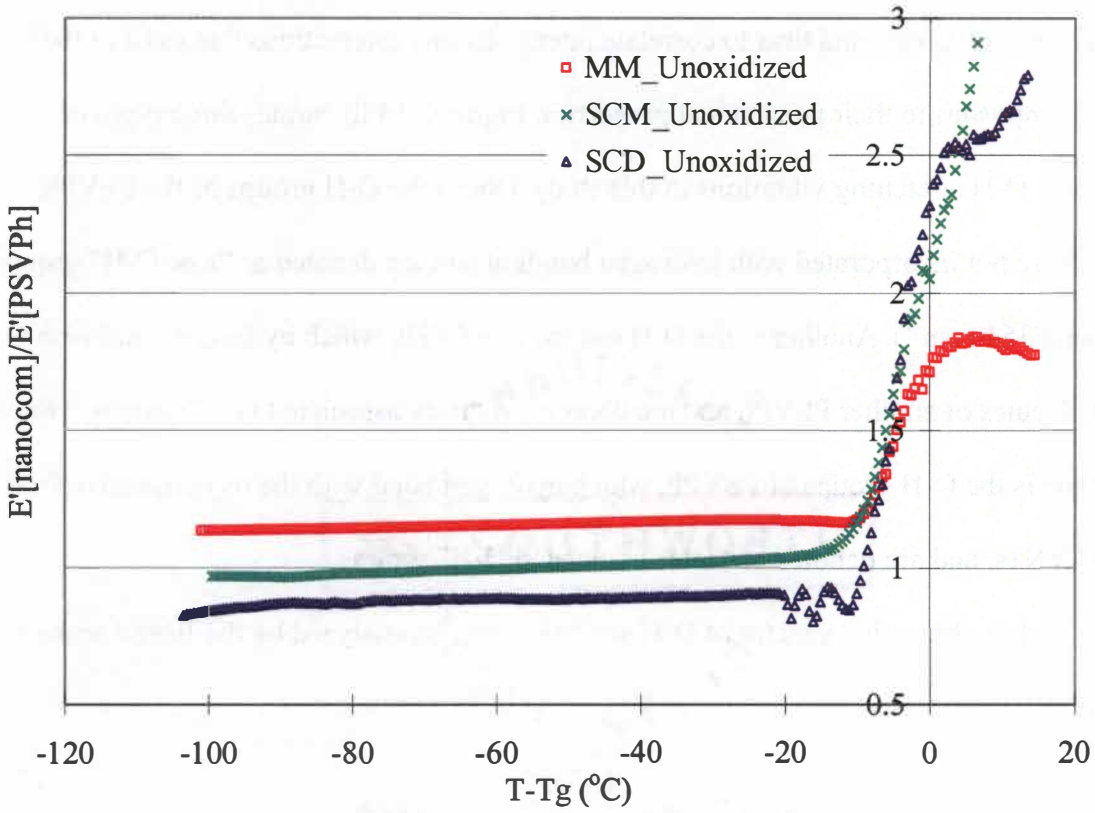

Figure 2.13 Summary of storage modulus ratio of nanocomposites with unoxidized MWNTs from MM, SCM, or SCD.

nanocomposites and PSVPh to quantify the intermolecular hydrogen bonding between MWNTs and PSVPh and thus to correlate intermolecular interactions that exist in the nanocomposites to their mechanical properties. Figure 2.14 illustrates three types of possible O-H stretching vibrations in this study. One is the O-H groups of the PSVPh, which are not incorporated with hydrogen bonding and are denoted as "free O-H" groups (around 3540 cm^{-1}). Another is the O-H groups of PSVPh, which hydrogen bond with O-H molecules of another PSVPh and are denoted as "intra-associated O-H" groups. The last one is the O-H groups of PSVPh, which hydrogen bond with the oxygenated defects of MWNTs, and are denoted as "inter-associated O-H" groups.

The absorption spectra of O-H stretching can be analyzed by the Beer-Lambert law:

$$A = abC \tag{2.6}$$

where A is the absorbance intensity of a specific band, a is the absorption coefficient of a specific band, and b is sample thickness, C is the concentration of specific functional groups present in the sample.[46] In this study, the ratio of the concentration of the free O-H ($C_{F,\text{-}OH}$), intra-associated O-H ($C_{A,\text{-}OH}$), and inter-associated O-H ($C_{I,\text{-}OH}$) to the concentration of the total O-H ($C_{T,\text{-}OH}$) were determined to quantitatively study the extent of intermolecular hydrogen bonding between MWNTs and PSVPh. The concentration of total O-H vibration refers to the sum of the three different types of O-H vibrations in a nanocomposite system, and is expressed as the following equation:

$$C_{T,OH} = C_{F,OH} + C_{A,OH} + C_{I,OH} \tag{2.7}$$

First, $C_{T,\text{-}OH}$ in equation 2.7 can be calculated:

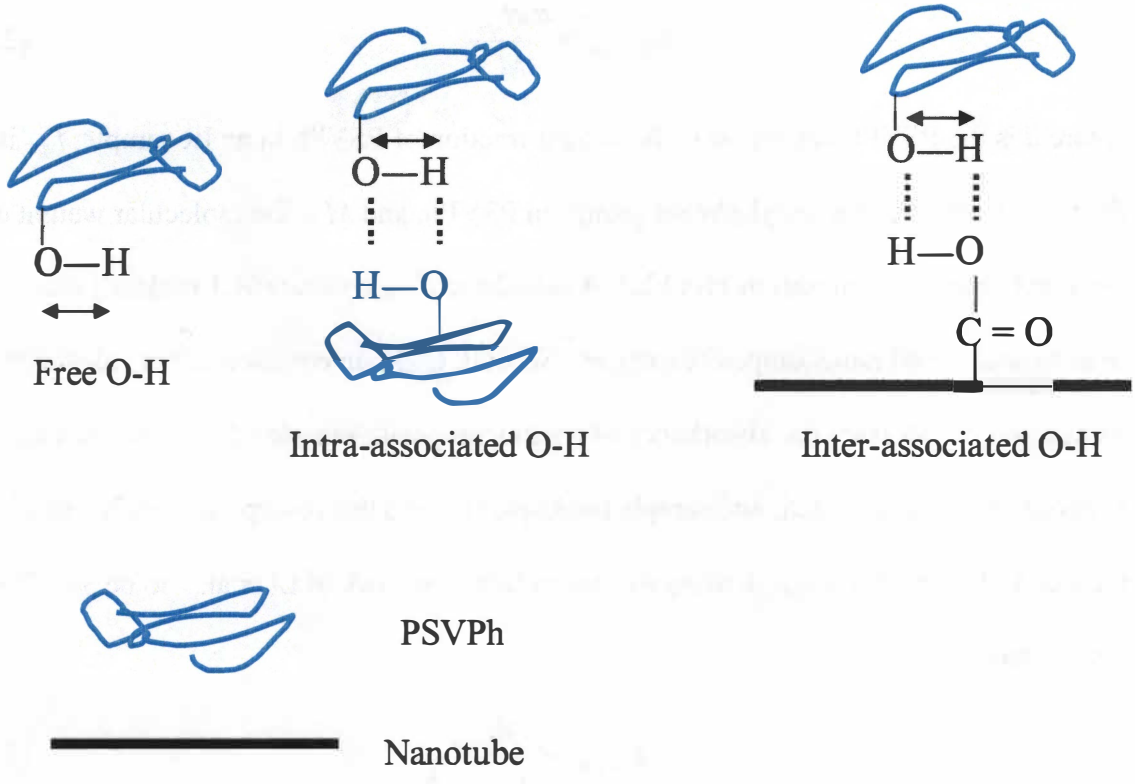

Figure 2.14 Scheme of possible O-H stretching vibrations in this study.

$$C_{T,-OH} = \frac{dwf_{vph}}{M} \tag{2.8}$$

where d is the PSVPh density, w is the weight fraction of PSVPh in an IR sample, f_{vph} is the mole fraction of the vinyl phenol groups in PSVPh, and M is the molecular weight of the vinyl phenol repeat unit in PSVPh.[36] A calculated $C_{T,-OH}$ value (64.1 mol/m^3) was used to analyze all nanocomposite samples. Second, $C_{F,-OH}$ in equation 2.7 is calculated from equation 2.6 from the absorbance of a nanocomposite sample ($A_{F,OH}$), which was experimentally determined, and sample thickness (b), and the absorption coefficient of the free O-H vibration ($a_{F,OH}$). $a_{F,OH}$ was taken from the work of Li et al.[47] to be 343.768 cm^{-1}m^2/mol.

$$C_{F,OH} = \frac{A_{F,OH}}{a_{F,OH} \times b} \tag{2.9}$$

Third, $C_{A,OH}$ and $C_{I,OH}$ were calculated from the following two equations. The first equation can be obtained by rewriting equation 2.7 as the following:

$$C_{A,OH} + C_{I,OH} = C_{T,OH} - C_{F,OH} \tag{2.10}$$

Since $C_{T,OH}$ and $C_{F,OH}$ were calculated from equation 2.8 and 2.9 respectively, the left hand side of equation 2.10 is known. The second equation can be obtained from equation 2.6:

$$C_{I,OH} = \frac{A_{A,OH}}{a_{asso,OH} \times b} \ , \ C_{A,OH} = \frac{A_{I,OH}}{a_{asso,OH} \times b} \tag{2.11}$$

where $a_{asso,OH}$ refers to intra- or inter-associated O-H absorption coefficient, and b is the same sample thickness. In this study, it is assumed that the absorption coefficient of intra-associated O-H and inter-associated O-H are the same. Based on this assumption and

equation 2.11, the ratio of $C_{I,OH}$ to $C_{A,OH}$ is equal to the ratio of $A_{A,OH}$ to $A_{I,OH}$, and this relation is expressed as the following:

$$\frac{C_{I,OH}}{C_{A,OH}} = \frac{A_{I,OH}}{A_{A,OH}} \tag{2.12}$$

Since $A_{A,OH}$ and $A_{I,OH}$ were experimentally determined, the ratio of $A_{I,OH}$ to $A_{A,OH}$ are also known values. From equation 2.10 and 2.12, $C_{I,OH}$ and $C_{A,OH}$ can be determined. Finally, the ratio of $C_{F,OH}$ (equation 2.9), $C_{A,OH}$, and $C_{I,OH}$ (equation 2.10 and 2.12) to $C_{T,OH}$ (equation 2.8) were calculated. However, it should be noted that the calculated $C_{A,OH}$ and $C_{I,OH}$ values cannot be taken as absolute values since it was assumed that the absorption coefficients of intra- and inter-associated OH vibration are identical, an assumption that has not been verified.[36] These values, however, could be used to compare the relative amounts of intra- or inter-associated OH in the nanocomposite samples in this study.

The absorbance of each OH vibration in the nanocomposites was determined from the IR peaks. The free, intra-associated, and inter-associated O-H peaks were deconvoluted using Peakfit software (v 4.12). The position and width of the free OH and intra-associated OH peaks were fixed with the peak position and width determined from the PSVPh sample. However, the position and width of inter-associated OH peak were allowed to float in the fitting procedure.

Figure 2.15 shows an example of the peak-fitted curves of the MM_Oxidized nanocomposite IR data. Table 2.2 shows the summary of the curve-fitting results for the nanocomposites prepared from the three different sample preparation processes with oxidized or unoxidized MWNTs. Additionally, Figure 2.16 (a) and (b) show the ratio of concentration of free ($C_{F,OH}$), intra-associated ($C_{A,OH}$) and inter-associated ($C_{I,OH}$) OH

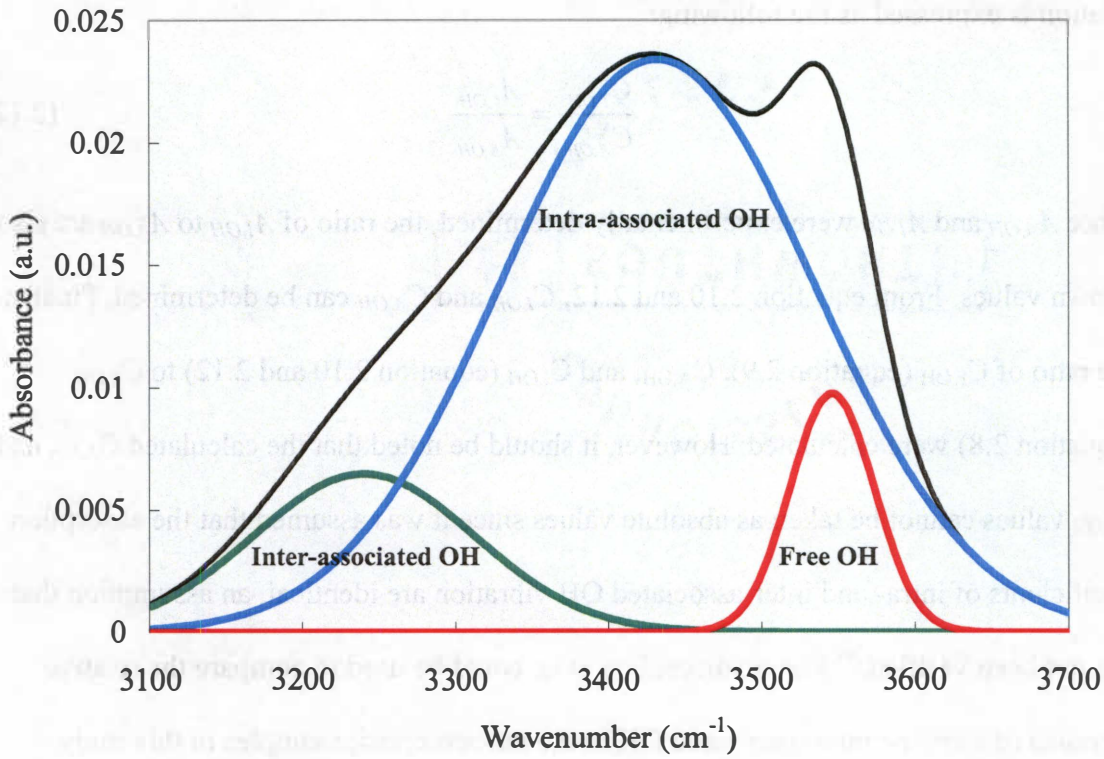

Figure 2.15 Example of peak-fitted curves of a MM_Oxidized nanocomposite.

Table 2.2 Summary of peak-fitting results for nanocomposites from three different sample preparation procedures.

	Free OH				Intra-associated OH				Inter-associated OH						
	ν^* (cm^{-1})	$W_{1/2}$*	$A_{F,OH}$ (cm^{-1})	$C_{F,OH}$	ν^* (cm^{-1})	$W_{1/2}$*	$A_{A,OH}$ (cm^{-1})	$C_{A,OH}$	ν^* (cm^{-1})	$W_{1/2}$	$A_{I,OH}$ (cm^{-1})	$C_{I,OH}$	$C_{F,OH}$ /$C_{T,OH}$	$C_{A,OH}$ /$C_{T,OH}$	$C_{I,OH}$ /$C_{T,OH}$
MM_Oxidized	3546	27.5	0.67 ± 0.02	4.98 ± 0.05	3432	103	6.04 ± 0.05	49.5 ± 2	3240	72.8	1.18 ± 0.04	9.66 ± 0.01	0.078 ± 0.003	0.77 ± 0.04	0.151 ± 0.005
MM_Unoxidized	3546	27.5	1.44 ± 0.02	10.7 ± 0.05	3432	103	6.39 ± 0.05	50.8 ± 2	3221	45.7	0.32 ± 0.04	2.55 ± 0.01	0.167 ± 0.005	0.79 ± 0.04	0.039 ± 0.001
SCM_Oxidized	3546	27.5	0.83 ± 0.02	6.17 ± 0.05	3432	103	5.27 ± 0.05	54.4 ± 2	3236	43.5	0.34 ± 0.04	3.51 ± 0.02	0.096 ± 0.003	0.85 ± 0.04	0.055 ± 0.002
SCM_Unoxidized	3546	27.5	2.35 ± 0.04	17.5 ± 0.1	3432	103	8.57 ± 0.08	43.7 ± 2	3223	55.2	0.57 ± 0.07	2.91 ± 0.02	0.272 ± 0.008	0.68 ± 0.03	0.045 ± 0.001
SCD_Oxidized	3546	27.5	0.97 ± 0.02	7.21 ± 0.05	3432	103	5.47 ± 0.05	52.0 ± 2	3236	52.6	0.51 ± 0.04	4.85 ± 0.01	0.112 ± 0.004	0.81 ± 0.04	0.076 ± 0.002
SCD_Unoxidized	3546	27.5	1.86 ± 0.04	13.8 ± 0.1	3432	103	9.86 ± 0.08	46.7 ± 2	3236	55.9	0.74 ± 0.06	3.51 ± 0.01	0.216 ± 0.007	0.73 ± 0.04	0.055 ± 0.002

* Values were fixed during curve-fitting.

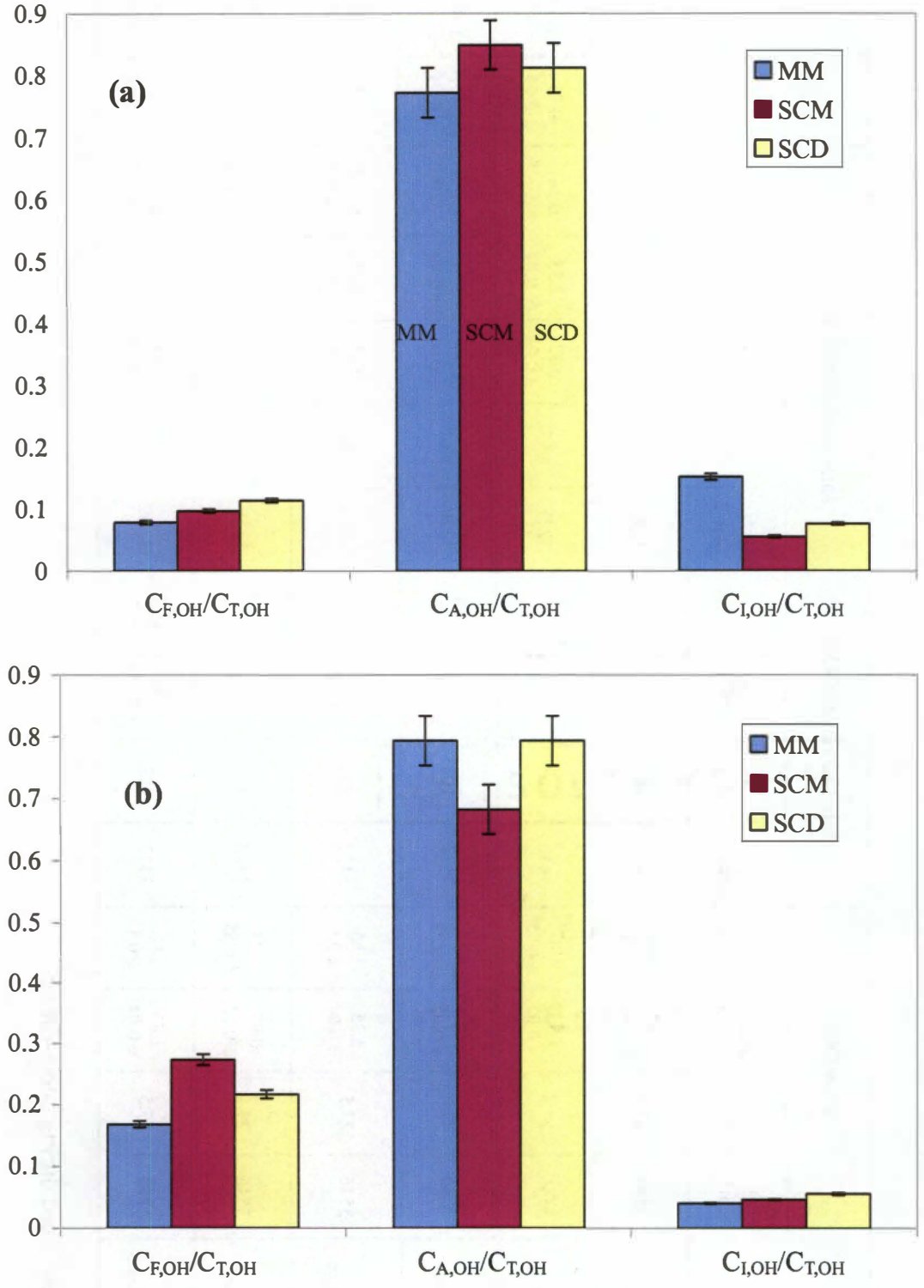

Figure 2.16 The ratio of concentration of free ($C_{F,OH}$), intra-associated ($C_{A,OH}$) and inter-associated ($C_{I,OH}$) to that of total OH ($C_{T,OH}$) vibration for nanocomposites with (a) oxidized and (b) unoxidized MWNTs.

vibration to that of total ($C_{T,OH}$) OH vibration in the nanocomposites with (a) oxidized and (b) unoxidized MWNTs. As can be seen in Table 2.2 and Figure 2.16 (a), the amount of inter-associated OH is highest for the melt-mixed nanocomposites with oxidized MWNTs. Additionally, the free and intra-associated OH is lowest for the melt-mixed nanocomposites with oxidized MWNTs. This suggests that the melt-mixing is most effective at the formation of intermolecular hydrogen bonding between MWNTs and polymers.

To correlate the results of IR analysis with the mechanical properties of nanocomposites, the E' ratio of MM, SCM, or SCD samples with oxidized or unoxidized MWNTs is plotted as a function of the ratio of $C_{I,OH}$ to $C_{T,OH}$ as shown in Figure 2.17. E' was estimated by averaging the E' ratio of each nanocomposite over $-60\,^{\circ}C < T - Tg < -40\,^{\circ}C$. As can be seen in Figure 2.17, the highest E' ratio is present in the melt-mixed nanocomposite with oxidized MWNTs, which correlates to the most inter-associated OH. This data suggests that the higher modulus of the melt-mixed nanocomposites may be correlated to the formation of more intermolecular hydrogen bonding than in solution-cast nanocomposites. More specifically, melt-mixing appears to be a very effective sample preparation procedure to optimize the formation of intermolecular interactions between MWNTs and polymers, and thus leads to improved mechanical properties of the final polymer carbon nanotube nanocomposites. Additionally, when the E' ratio of the nanocomposites with oxidized or unoxidized MWNTs prepared by identical sample preparation procedures are compared, the E' ratio of the nanocomposites with oxidized MWNTs is higher than that of nanocomposites with unoxidized MWNTs. This also suggests that the formation of more intermolecular hydrogen bonding leads to improved

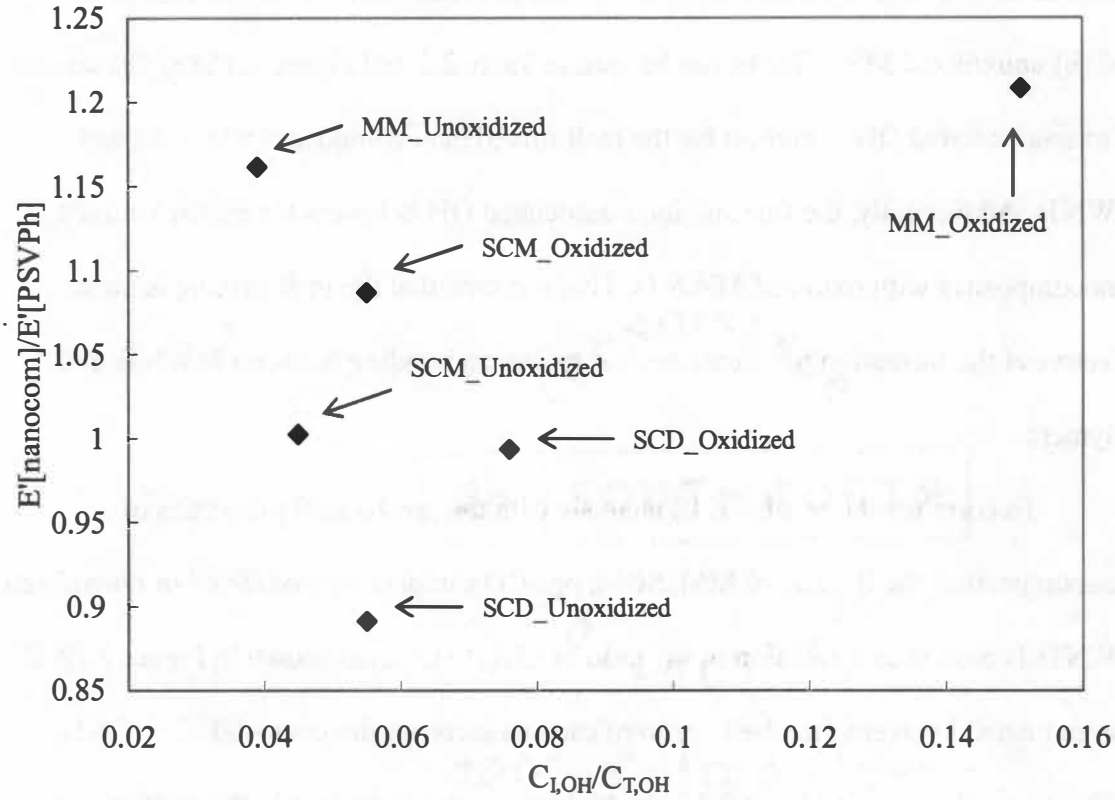

Figure 2. 17 Storage modulus ratio (♦) of MM, SCM, or SCD samples with oxidized or unoxidized MWNTs normalized to that of the PSVPh as a function of the ratio of concentration of inter-associated ($C_{I,OH}$) to that of total OH ($C_{T,OH}$) vibration.

mechanical properties of the nanocomposites.

2.3 Conclusions

In this study, the impact of sample preparation processes on polymer CNT nanocomposites was examined by measuring the dynamic mechanical properties of PSVPh/MWNT nanocomposites, and quantifying the extent of intermolecular hydrogen bonding between the MWNTs and the polymers with IR. The DMA data suggests that melt-mixing leads to more stable state of the nanocomposite morphology, which maybe due to the "wrapping" of MWNTs with polymers during processing at high temperature, which is not observed for solution casting. Additionally, DMA data suggests that melt-mixing results in more improvement of the mechanical properties of the nanocomposite than solution casting. Furthermore, the IR data analysis shows that the melt-mixing forms more intermolecular hydrogen bonding. Therefore, this study can be used as a guideline to achieve improved morphologies and properties of polymer carbon nanotube nanocomposites by optimizing intermolecular interactions between nanotubes and polymers using processing.

CHAPTER 3

SEQUESTERING SURFACE-MODIFIED GOLD NANOPARTICLES IN DIBLOCK COPOLYMERS: STARTING MATERIALS

3.1 Experimental

3.1.1 Synthesis of Thiol-terminated Polystyrene

Thiol-terminated polystyrene (PS-SH) with low molecular weight was synthesized starting with bromine-terminated polystyrene (PS-Br), which was synthesized via ATRP, followed by thiolation of PS-Br to PS-SH. This synthesis procedure was developed to modify the process reported by Garamszegi et al.[48] All chemicals in this reaction were purchased from Aldrich, and used as received. In a typical procedure for the synthesis for PS-Br, styrene (monomer, 10 g, 96 mmol, 4.8 equiv.), copper (I) bromide (CuBr, catalyst, 2.869 g, 20 mmol, 1 equiv.), 1-phenylethyl bromide (1-PEBr, initiator, 3.7014g, 20mmol, 1 equiv.), N,N,N',N',N''-pentamethyldiethylenetriamine (PMDETA, ligand, 6.932g, 40mmol, 2 equiv.) and anhydrous THF (solvent, 10 g) were added to a 100 ml two-neck, round-bottom flask. All reactants were degassed through freeze-thaw processes that were repeated five times. The polymerization was conducted under argon in an oil bath at 110 °C for 90 min. After polymerization, the polymers were purified by dissolving in THF and precipitating in cold methanol. This process was repeated three times. The resultant polymers were then dried under vacuum at 50 °C for 24 hrs. The purified polymers were characterized by GPC to measure molecular weight and by NMR for end group analysis.

The thiolation of PS-Br was conducted to convert the bromine-end groups to

thiol-end groups. In a typical thiolation reaction, PS-Br (1 g, 0.89 mmol, 1 equiv.) was completely dissolved in 30 ml of DMF, and thiourea (0.68 g, 8.9 mmol, 10 equiv.) was then added to this polymer/DMF solution. This mixture was stirred under argon at 100 °C for 24 hrs. NaOH (sodium hydroxide, 0.36 g, 8.9 mmol, 10 equiv.) dissolved in 2.9 ml of water was then added, and this mixture was heated at 110 °C for another 24 hrs. Seven drops of 95 % sulfuric acid mixed with 1.8 ml of water were added and this mixture was stirred at room temperature for an additional 5 hrs. The polymers were then purified by dissolving in THF and precipitating in cold methanol and repeated twice. The final product was dried under vacuum at 50 °C for 24 hrs. The dried polymers were characterized by GPC and by NMR to verify the conversion of bromine end groups to thiol end groups. Figure 3.1 shows the scheme for the synthesis procedure for PS-SH starting with PS-Br.

3.1.2 Synthesis of Polystyrene-coated Gold Nanoparticles

Gold nanoparticles with surfaces that are coated with low molecular weight polystyrene (PS-coated Au nanoparticles) were synthesized by utilizing thiol-terminated polystyrene (PS-SH) as a stabilizing ligand during the synthesis. The success of this reaction is based on the fact that "a thiol ligand strongly binds gold due to the soft character of both Au and S."[49] This synthesis procedure was developed to mimic the process reported by Brust et al.[50] and Bockstaller et al.,[38,51] which is a two-phase synthesis procedure. In this reaction, hydrogen tetrachloroaurate(III) hydrate, sodium borohydride, and tetraoctylammonium bromide were purchased from Sigma-Aldrich, and used as received. An aqueous solution of hydrogen tetrachloroaurate ($HAuCl_4 3H_2O$, 35.4

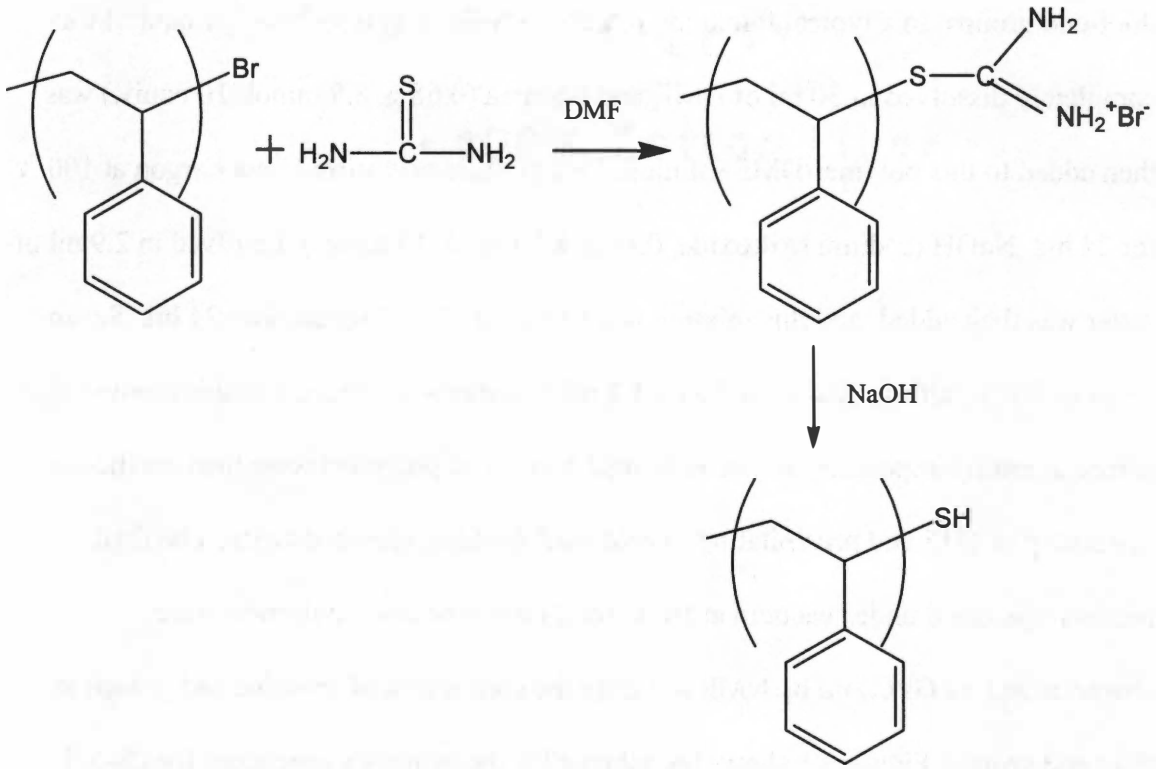

Figure 3.1 Scheme for synthesis procedure of PS-SH[48]

mg in 3 ml water, 30 mmol/L) was mixed with a solution of tetraoctylammonium bromide in toluene ($N(C_8H_{17})_4Br$, 218.7 mg in 8ml toluene, 50 mmol/L), which is a phase transfer agent in this reaction.[51] This mixture was vigorously stirred for 3 hrs until the tetrachloroaurate was completely transferred from the aqueous phase to the toluene layer, which can be verified by the appearance of the yellowish color of the toluene layer. The organic phase was separated from the two-phase (water/toluene) system. PS-SH (150 mg, 0.1 mmol) was then added to the separated toluene layer. An aqueous solution of sodium borohydride ($NaBH_4$, 37.8g in 2.5ml water, 0.4 mol/L), which is a reducing agent in this reaction, was gradually added while this mixture was vigorously stirring.[51] With the addition of sodium borohydride, a color change of the solution was observed from yellow to red-wine. This mixture was stirred for 3 hrs, and the organic phase was then separated. This separated solution was evaporated to 1 ml using a rotary evaporator. The final product was precipitated in a mixture of methanol and ethanol (1 : 1 in volume ratio), and the dark brown product was filtered.[38] Any unbound PS-SH ligands were removed by washing with a mixture of ethanol and THF (5 : 1) several times.[38] The final PS-coated gold nanoparticles were dried under vacuum at 70 °C for 24 hrs.

3.1.3 Transmission Electron Microscopy (TEM) of Gold Nanoparticles

The prepared gold nanoparticles were characterized by transmission electron microscope (TEM, Hitachi H800) with an acceleration voltage of 100 KeV. To examine the PS-coated gold nanoparticles by TEM, a dilute solution of the gold nanoparticles in toluene (5 mg/ml) was prepared. One drop of this solution was placed on porous carbon films supported by copper grids.[50] These films were dried in air to evaporate the solvent.

3.1.4 Synthesis of Bromine-terminated Poly(styrene-co-acetoxystyrene) Copolymers, and their Hydrolysis or Thiolation

In this study, the synthesis of thiol-terminated poly(styrene-co-vinyl phenol) copolymers (PSVPh-SH) was first attempted starting with synthesizing bromine-terminated poly(styrene-co-acetoxystyrene) copolymers via ATRP, and followed by hydrolysis or thiolation. In the synthesis of bromine-terminated poly(styrene-co-acetoxystyrene) copolymers, styrene (monomer, 8.6 g, 82 mmol, 4.1 equiv.), 4-acetoxystyrene (monomer, 2.2 g, 13 mmol, 0.67 equiv.), 1-phenylethylbromide (1-PEBr, initiator, 3.7 g, 20 mmol, 1 equiv.), copper (I) bromide (CuBr, catalyst, 2.9 g, 20 mmol, 1 equiv.), N,N,N',N',N"-pentamethyldiethylenetriamine (PMDETA, ligand, 6.9 g, 40 mmol, 2 equiv.), and anhydrous THF (solvent, 10.8 g) were added to two-neck, round bottom flask. All reactants were degassed by freeze and thaw repeated 3 times. Polymerization was then conducted in an oil bath at 110 °C for 90 mins. After 90 mins, polymers were purified by precipitating in cold methanol three times. Final products were filtered, and dried under vacuum at 75 °C for 24 hrs.

Additionally, hydrolysis of bromine-terminated poly(styrene-co-acetoxystyrene) copolymers was conducted as follows: 1 g of bromine-terminated poly(styrene-co-acetoxystyrene) copolymers was completely dissolved in 10 ml of dioxane, and 3 g of hydrazine hydrate was added to this polymer/dioxane solution. This mixture was stirred for 48 hrs at room temperature. Polymers were then precipitated in cold methanol, and dried under vacuum at 85 °C for 24 hrs.

Finally, thiolation of bromine-terminated poly(styrene-co-acetoxystyrene) copolymers was conducted as follows: 1 g of bromine-terminated poly(styrene-co-

acetoxystyrene) was completely dissolved in 30 ml of DMF. Thiourea (0.48 g, 6.3 mmol, 10 equiv.) was added to this polymer/DMF solution, and this mixture was stirred at 110 °C for 24 hrs. Five drops of 95 % sulfuric acid in 1.3 ml of water were then added, and this mixture was stirred at room temperature for an additional 5 hrs. The polymers were purified by precipitating in cold methanol repeated twice. Final products were dried under vacuum at 75 °C for 24 hrs.

3.1.5 Synthesis of Thiol-terminated Poly(styrene-co-vinyl phenol) Copolymers

The synthesis of thiol-terminated poly(styrene-co-vinyl phenol) (PSVPh-SH) copolymers was attempted by first synthesizing bromine-terminated poly(styrene-co-4-tert-butoxystyrene) copolymers via ATRP, followed by the thiolation of the copolymers to thiol-terminated poly(styrene-co-4-tert-butoxystyrene) copolymers, and the subsequent hydrolysis of the thiol-terminated poly(styrene-co-4-tert-butoxystyrene) to PSVPh-SH. Figure 3.2 shows the proposed scheme for the synthesis for thiol-terminated poly(styrene-co-vinyl phenol) copolymers. In a typical synthesis of the bromine-terminated poly(styrene-co-4-tert-butoxystyrene), styrene (23.9 g, 230.4 mmol, 3.8 equiv.), 4-tert-butoxystyrene (10.2 g, 57.6 mmol, 0.96 equiv.), copper (I) bromide (8.6 g, 60 mmol, 1 equiv.), 1-phenylethyl bromide (1-PEBr) (11.1 g, 60 mmol, 1 equiv.), N,N,N',N',N"-pentamethyldiethylenetriamine (PMDETA) (20.8 g, 120 mmol, 2 equiv.), and anhydrous THF (34.2 g) were added to a two-neck, round bottom flask. All reactants were degassed by freeze-thaw techniques repeated 7 times. The polymerization was conducted under argon in an oil bath at 110 °C for 90 mins. After 90 mins, the flask was immediately

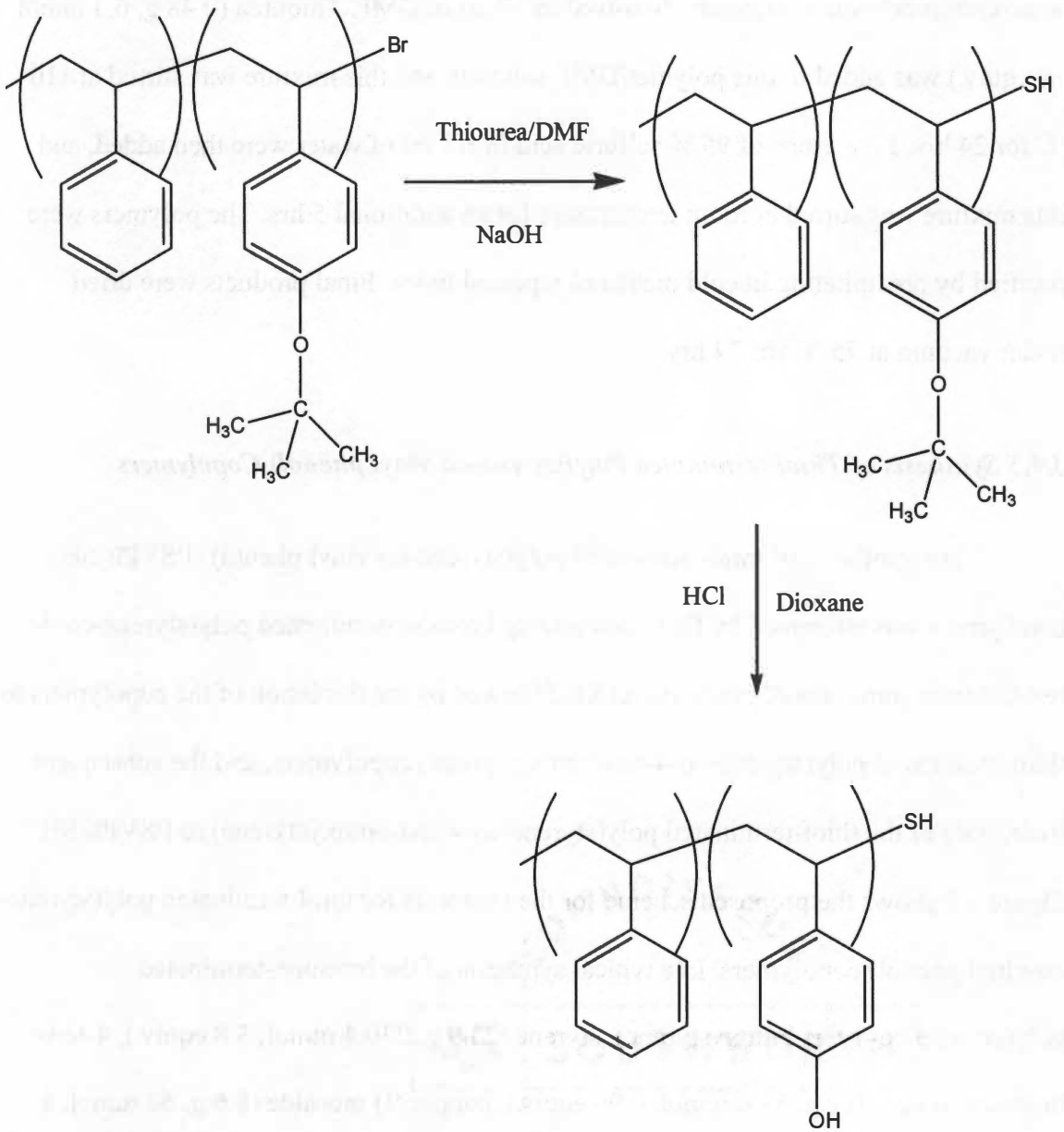

Figure 3.2 Scheme for synthesis procedures for thiol-terminated poly(styrene-co-vinyl phenol) copolymers starting with bromine-terminated poly(styrene-co-4-tert-butoxystyrene) copolymers.

opened, and the polymers were precipitated in cold methanol. The final product was filtered, and dried under vacuum at 50 °C for 24 hrs. The polymers were then characterized by GPC to determine molecular weight properties and by NMR to analyze the composition and verify the end capping of the copolymer.

The thiolation of the bromine-terminated poly(styrene-co-4-tert-butoxystyrene) copolymers was conducted by the following procedure: bromine-terminated poly(styrene-co-4-tert-butoxystyrene) (0.29 g, 0.21 mmol, 1 equiv.) was completely dissolved in 8.7 ml of DMF, and thiourea (0.16 g, 2.05 mmol, 10 equiv.) was then added into this polymer/DMF solution. This mixture was vigorously stirred under argon at 100 °C for 24 hrs. NaOH (0.082 g, 2.05 mmol, 10 equiv.) dissolved in 0.7 ml of water was then added, and this mixture was stirred at 110 °C under argon for 24 hrs. Two drops of 95 % sulfuric acid in 0.41 ml water were added, and this mixture was stirred at room temperature for an additional 5 hrs. The polymers were precipitated in cold methanol, and filtered. Final polymer products were dried under vacuum at 50 °C for 24 hrs. After thiolation, polymers were characterized by GPC, and by NMR to confirm the conversion of bromine-end groups to thiol-end groups.

The hydrolysis of the thiol-terminated poly(styrene-co-4-tert-butoxystyrene) copolymers was developed from the work reported by Asari et al.[52], where the synthesis procedures are: 70 mg of thiol-terminated poly(styrene-co-4-tert-butoxystyrene) was completely dissolved in dioxane, and this polymer solution was kept under argon for 15 mins at 80 °C. Five drops of conc. hydrochloric acid (HCl) was added to this mixture, and it was stirred under argon for 30 mins. The polymers were then precipitated in cold methanol, and filtered. Final products were dried under vacuum at 50 °C for 24 hrs. After

hydrolysis, the polymers were characterized by GPC, and by NMR to analyze thiol-end groups and to confirm the conversion of tert-butoxy groups to hydroxyl groups.

3.2 Results and Discussion

3.2.1 Bromine-terminated Polystyrene

Atom transfer radical polymerization (ATRP) is a controlled free radical polymerization.[43] In a typical ATRP reaction, a halogen atom at the end of a polymer is transferred to a Cu(I) complex to allow the reaction with monomer to grow the polymer chain, and the halogen atom can also return to the polymer chain end to limit radical concentration, and thus termination.[43,48] Thus, polymers, at which end a halogen atom exists, with controlled polydispersities can be synthesized via ATRP.[43,48] In this study, bromine-terminated polystyrene with low polydispersity was synthesized by ATRP. The molecular weight characteristics of bromine-terminated polystyrene (PS-Br) was found to have an Mn of 1,100 g/mol, Mw of 1,300 g/mol, and PDI of 1.18. This GPC data indicates that the molecular weight of polymers can be controlled by manipulating the ratio of monomer, catalyst, initiator, and ligand and by adding solvent (THF in this study) in ATRP. Specifically, the ratio, 4.8: 1: 1: 2 of monomer (styrene, 4.8 equiv.), catalyst (CuBr, 1 equiv.), initiator (1-PEBr, 1 equiv.) and ligand (PMDETA, 2 equiv.) and the same amount of solvent as that of monomers provide low molecular weight of polymers and low polydispersity.

These experimental results were obtained as the following: first, the amount of monomers, initiator, catalyst, and ligand to synthesize bromine-terminated polystyrene with a target molecular weight (Mn) of 1,000 g/mol was calculated based on the fact that

the average degree of polymerization (DP) of polymers synthesized by living polymerization is the ratio of concentration of monomers to the concentration of initiators. That is, DP in a living polymerization is

$$DP = \frac{[M]_0}{[I]_0} \tag{3.1}$$

where $[M]_0$ is the concentration of monomers, and $[I]_0$ is the concentration of initiators.[43] More specifically, to obtain an Mn of 1,000 g/mol (DP = 9.6) of polystyrene, the expected mole ratio of monomers to initiators is 9.6 to 1 based on the equation 3.1. Therefore, the ratio, 9.6: 1: 1: 2 of monomers, initiators, catalysts, and ligands was first utilized in ATRP. This ratio of initiator, catalysts, and ligands, 1: 1: 2, was developed to mimic the process reported by Garamszegi et al.[48] The molecular weight of polystyrene in this first attempt was found to have an Mn of 3,500 g/mol, Mw of 5,100 g/mol, and PDI of 1.45. These molecular weight properties and polydispersity were higher than what was expected from the stoichiometric calculation. Therefore, to reach the target molecular weight of polystyrene via ATRP, the amount of initiators, catalysts, and ligands was doubled keeping the amount of monomers same. That is, the ratio, 4.8: 1: 1: 2 of monomers, initiators, catalysts, and ligands were utilized in this second attempt. The molecular weight of this polymer was found to have an Mn of 3,100 (g/mol), Mw of 5,100 (g/mol) and PDI of 1.65. This molecular weight is still higher than the target molecular weight (1,000 g/mol). Finally, solvent (anhydrous THF) with the same amount of monomers was added to the reactants with the ratio of 4.8: 1: 1: 2 of monomers, initiators, catalysts, and ligands. The molecular weight of polymer in this third attempt was found to have an Mn of 1,100 g/mol, Mw of 1,300 g/mol, and PDI of 1.18. This molecular weight of the

polymers is close to the target molecular weight (1,000 g/mol). Therefore, these experimental results provide a guideline to synthesize low molecular weight polymers by ATRP.

Additionally, NMR was utilized to analyze the bromine-end groups of the PS-Br. Figure 3.3 shows the ^{1}H spectrum of the bromine-terminated polystyrene dissolved in deuterated chloroform. As can be seen in Figure 3.3, "the methine proton next to the bromine chain end has a chemical shift of 4.45 – 4.75 ppm,"[48] which indicates that the bromine group at the end of the polymer chain exists.

3.2.2 Thiol-terminated Polystyrene

The molecular weight of thiol-terminated polystyrene (PS-SH) was also determined using a PC-GPC 120, and was found to have an Mn of 1,500, Mw of 1,800 and PDI of 1.20. Additionally, NMR was utilized to analyze thiol-end groups of the PS-SH. Figure 3.4 shows the ^{1}H spectrum of the thiol-terminated polystyrene dissolved in deuterated chloroform. As can be seen in Figure 3.4, the methine proton next to the thiol end groups has a chemical shift of 3.0 – 3.3 ppm, and the methine proton next to the bromine chain ends, as shown in Figure 3.3, disappears. This NMR data indicates that the conversion of the bromine-end groups to thiol-end groups was successful.

3.2.3 Polystyrene-coated Gold Nanoparticles

TEM is a useful tool to characterize the size distribution of nanoparticles. The primary contrast mechanism of TEM is based on the difference of electron density from different atoms.[53] The atoms of metal or semiconductor nanoparticles have much higher

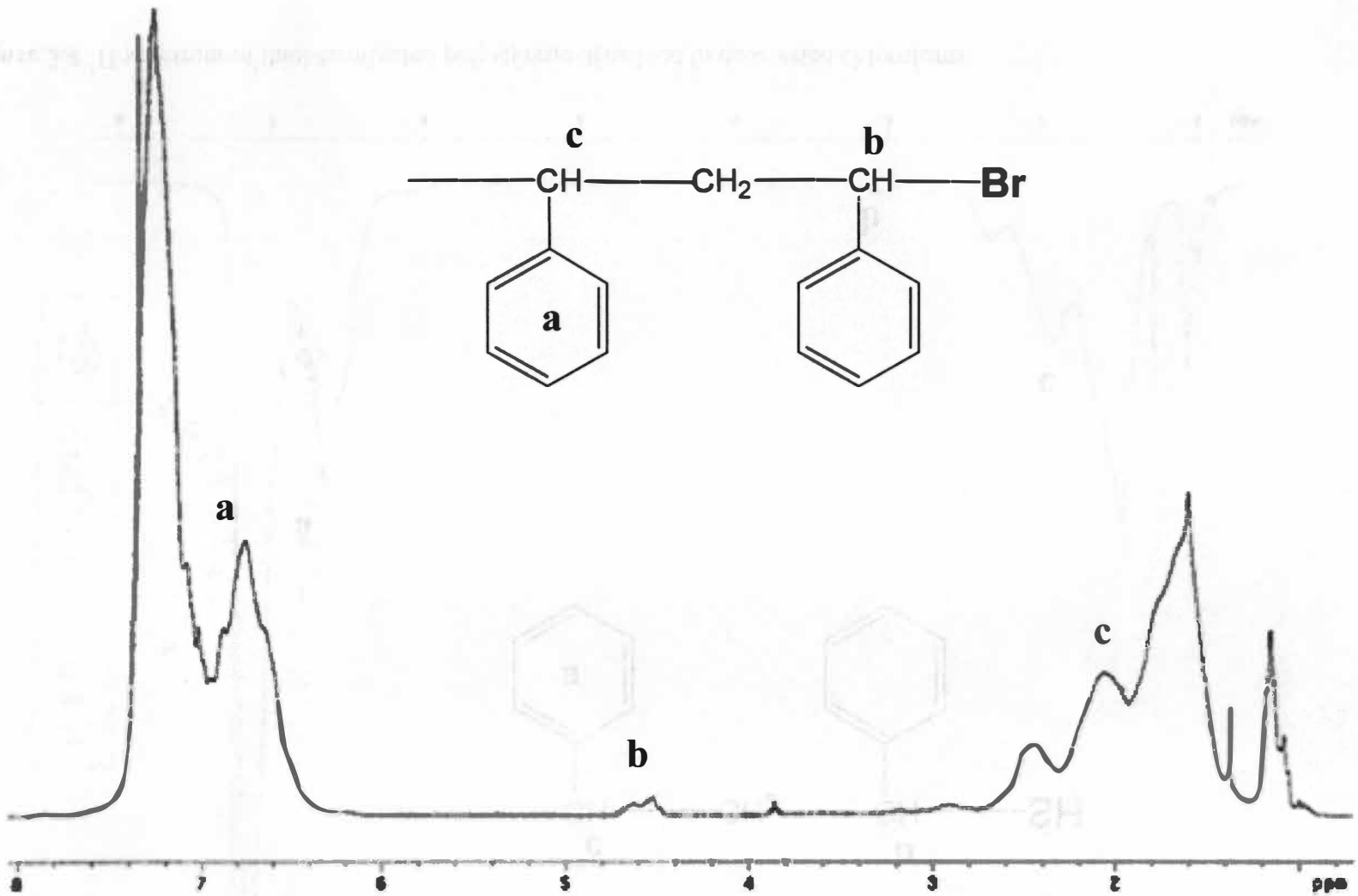

Figure 3.3 ^{1}H spectrum of bromine-terminated polystyrene dissolved in deuterated chloroform.

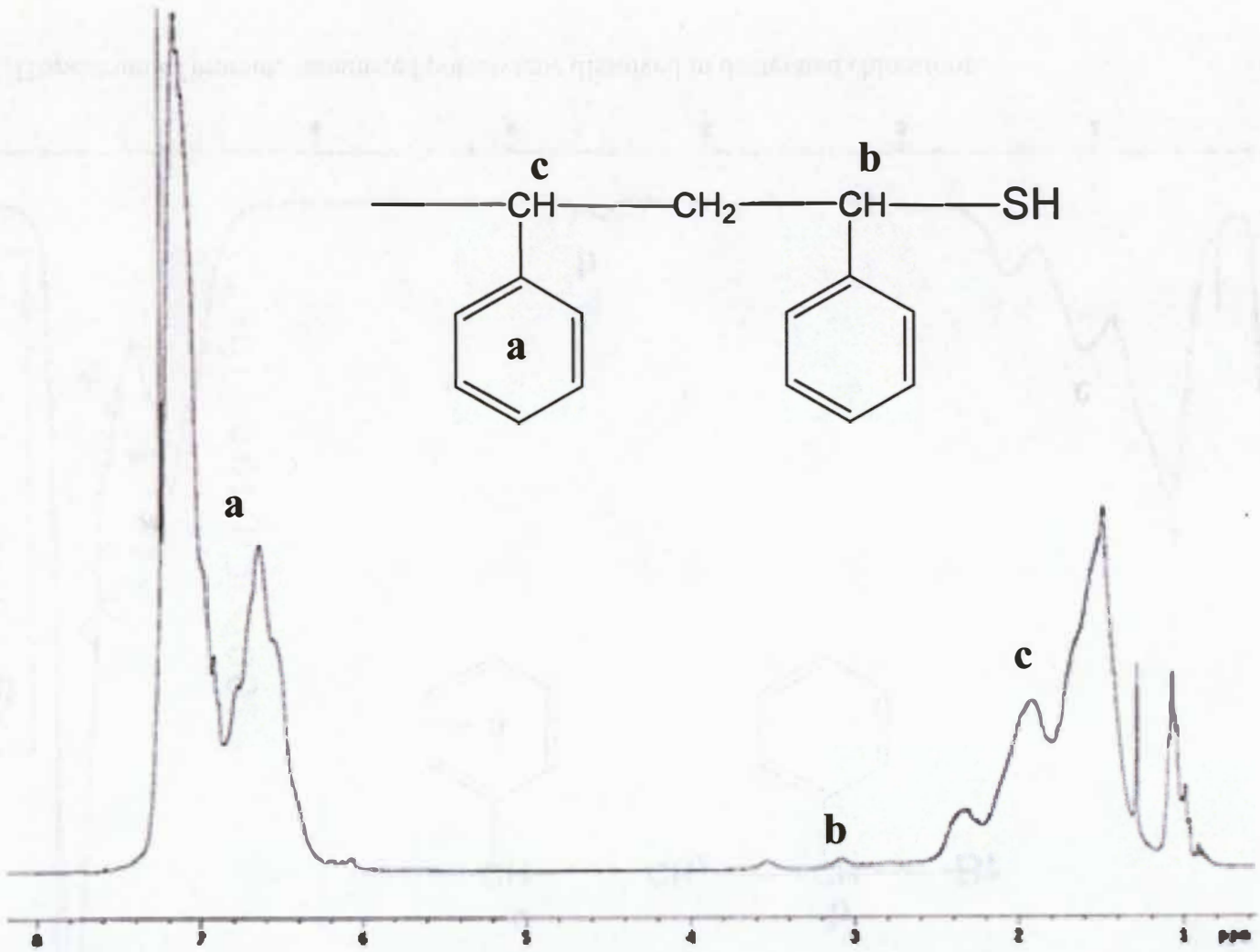

Figure 3.4 ^{1}H spectrum of thiol-terminated polystyrene dissolved in deuterated chloroform.

electron density than atoms of polymers. Thus, it is possible to obtain images of distribution of nanoparticles dispersed in polymers, which can be identified as dark spots in TEM images.[51] Additionally, a real space image can be obtained directly by TEM.[51] In this study, the polystyrene-coated gold nanoparticles were characterized by TEM to analyze the size and size distribution of the gold nanoparticles. Figure 3.5 shows the TEM images of the PS-coated gold nanoparticles synthesized in this project. Additionally, Figure 3.6 shows the size and size distribution of the gold nanoparticles, which were determined using Image J software (1.34 s) by counting 139 particles, and an average diameter was determined from this data to be 6.5 nm with standard deviation of 2.8. As can be seen Figure 3.5 and 3.6, the size of gold nanoparticles was controlled with the presence of thiol-terminated polystyrene, as it prevents the aggregation of gold nanoparticles.[15]

3.2.4 Attempt for Synthesis of Thiol-terminated Poly(styrene-co-vinyl phenol) Copolymers Starting with Bromine-terminated Poly(styrene-co-acetoxystyrene) Copolymers

In this study, the synthesis of thiol-terminated poly(styrene-co-vinyl phenol) copolymers was first attempted starting with bromine-terminated poly(styrene-co-acetoxystyrene) copolymers. Bromine-terminated poly(styrene-co-acetoxystyrene) copolymers were synthesized via ATRP, and both the hydrolysis and the thiolation of the copolymers were separately attempted. The molecular weight of the bromine-terminated poly(styrene-co-acetoxystyrene) copolymers was found to have an Mn of 1,600, Mw of 2,000, and PDI of 1.25. The bromine-end group and acetoxystyrene group of the copolymers were characterized by NMR. NMR data of bromine-terminated poly(styrene-

Figure 3.5 Representative TEM image of PS-coated gold nanoparticles. (Scale bar size: 100 nm)

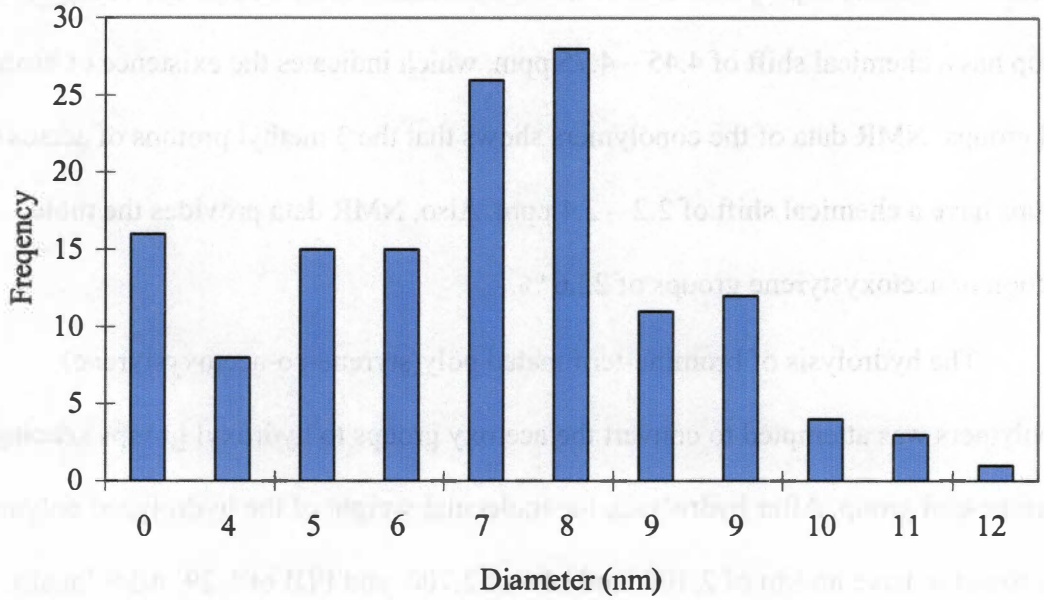

Figure 3.6 Size and size distribution of PS-coated gold nanoparticles.

co-acetoxystyrene) copolymers shows that the methine proton next to the bromine-end group has a chemical shift of 4.45 – 4.75 ppm, which indicates the existence of bromine-end groups. NMR data of the copolymers shows that the 3 methyl protons of acetoxy groups have a chemical shift of 2.2 – 2.4 ppm. Also, NMR data provides the mole fraction of acetoxystyrene groups of 22.6 %.

The hydrolysis of bromine-terminated poly(styrene-co-acetoxystyrene) copolymers was attempted to convert the acetoxy groups to hydroxyl groups keeping the bromine-end group. After hydrolysis, the molecular weight of the hydrolyzed polymers was found to have an Mn of 2,100, and Mw of 2,700, and PDI of 1.29. Additionally, NMR was utilized to analyze the bromine-end groups and to confirm the conversion of the acetoxy groups to hydroxyl groups. NMR data shows that the peak of the 3 methyl protons of the bromine-terminated poly(styrene-co-acetoxystyrene) copolymers at 2.2 – 2.4 ppm disappeared, which suggests the conversion of the acetoxy groups to hydroxyl groups. However, NMR data shows that clearly observed peaks of the methine proton next to the bromine-end group of the bromine-terminated poly(styrene-co-acetoxystyrene) copolymers become very weak after hydrolysis. This indicates that the hydrolysis using hydrazine hydrate alters the bromine-end groups, and may result in loss of the bromine-end groups. It was recognized that few bromine-end groups were not enough to create thiol-end groups.

The thiolation of the bromine-terminated poly(styrene-co-acetoxystyrene) copolymers was also attempted to convert the bromine-end groups of the copolymers to thiol-end groups while keeping the acetoxy groups. NMR was utilized to confirm the conversion of bromine-end groups of the copolymers to thiol-end groups, and to analyze

the acetoxy groups of the copolymers.

In the NMR data of the copolymers after thiolation, the peak of the methine proton next to the thiol-end group at 3.0 – 3.2 ppm was rarely observed. Additionally, a weak peak of the methine proton next to the bromine-end group was observed although the thiolation was conducted. This NMR data indicates that the thiolation of the bromine-terminated poly(styrene-co-acetoxystyrene) copolymers using thiourea was not successful, and may result in loss of the bromine-end groups of the copolymers. Additionally, NMR data shows that peaks of 3 methyl protons of the acetoxy groups in the bromine-terminated copolymers unexpectedly disappeared after thiolation, which indicates that the acetoxy groups of the bromine-terminated copolymers may be lost during thiolation. This NMR data suggests that acetoxy styrene groups, which have ester bonds, are not stable during thiolation using hydrazine hydrate and NaOH.

NMR data of the bromine-terminated poly(styrene-co-acetoxy styrene) copolymers after hydrolysis or thiolation suggests that bromine-terminated poly(styrene-co-acetoxystyrene) copolymers may not be appropriate as starting materials to synthesize thiol-terminated poly(styrene-co-vinyl phenol) copolymers. Therefore, in this study, the synthesis of thiol-terminated poly(styrene-co-vinyl phenol) copolymers was attempted starting with bromine-terminated poly(styrene-co-4-tert-butoxystyrene) copolymers, followed by thiolation and hydrolysis, which was selected in that the ether bonds of the tert-butoxystyrene groups may be more stable under thiolation than the ester bonds of the acetoxystyrene groups.

3.2.5 Bromine-terminated Poly(styrene-co-4-tert-butoxystyrene) Copolymers

The molecular weight of the bromine-terminated poly(styrene-co-4-tert-butoxystyrene) copolymers was determined by PL-GPC and to have an Mn of 1,412, Mw of 1,685, and PDI of 1.19. Additionally, NMR was utilized to analyze the bromine-end groups and composition of the copolymer. Figure 3.7 shows the ^{1}H spectrum of the bromine terminated poly(styrene-co-4-tert-butoxystyrene) copolymers dissolved in deuterated dioxane. As can be seen, the methine proton next to the bromine end group has a chemical shift of 4.45 – 4.75 ppm. This data indicates the presence of the bromine-end group of the copolymer. Additionally, based on the integration of proton groups, the composition of the copolymer was determined by analysis of these spectra. In this analysis, the mole fraction of styrene groups is set to x, and fraction of tert-butoxystyrene groups y. Based on the presence of 5 aromatic protons in each styrene group and 4 aromatic protons in each butoxystyrene group, the equation $5x + 4y = 9.21$ is valid, where 9.21 is the area of the aromatic (6.2 – 7.6 ppm) peaks in the NMR curve. Additionally, the integration of the 9 methyl protons in the tert-butoxy groups, which occurs 1.2 – 1.4 ppm,[54] provides the relationship $9y = 1$. Solving these 2 equations leads to the result that the mole fraction of tert-butoxystyrene in the copolymer is 5.9 %.

3.2.6 Thiol-terminated Poly(styrene-co-4-tert-butoxystyrene) Copolymers

The molecular weight of the thiol-terminated poly(styrene-co-4-tert-butoxystyrene) copolymers was determined by GPC, and found to have an Mn of 1,900 g/mol, Mw of 2,700 g/mol, and PDI of 1.42. Additionally, NMR was utilized to confirm

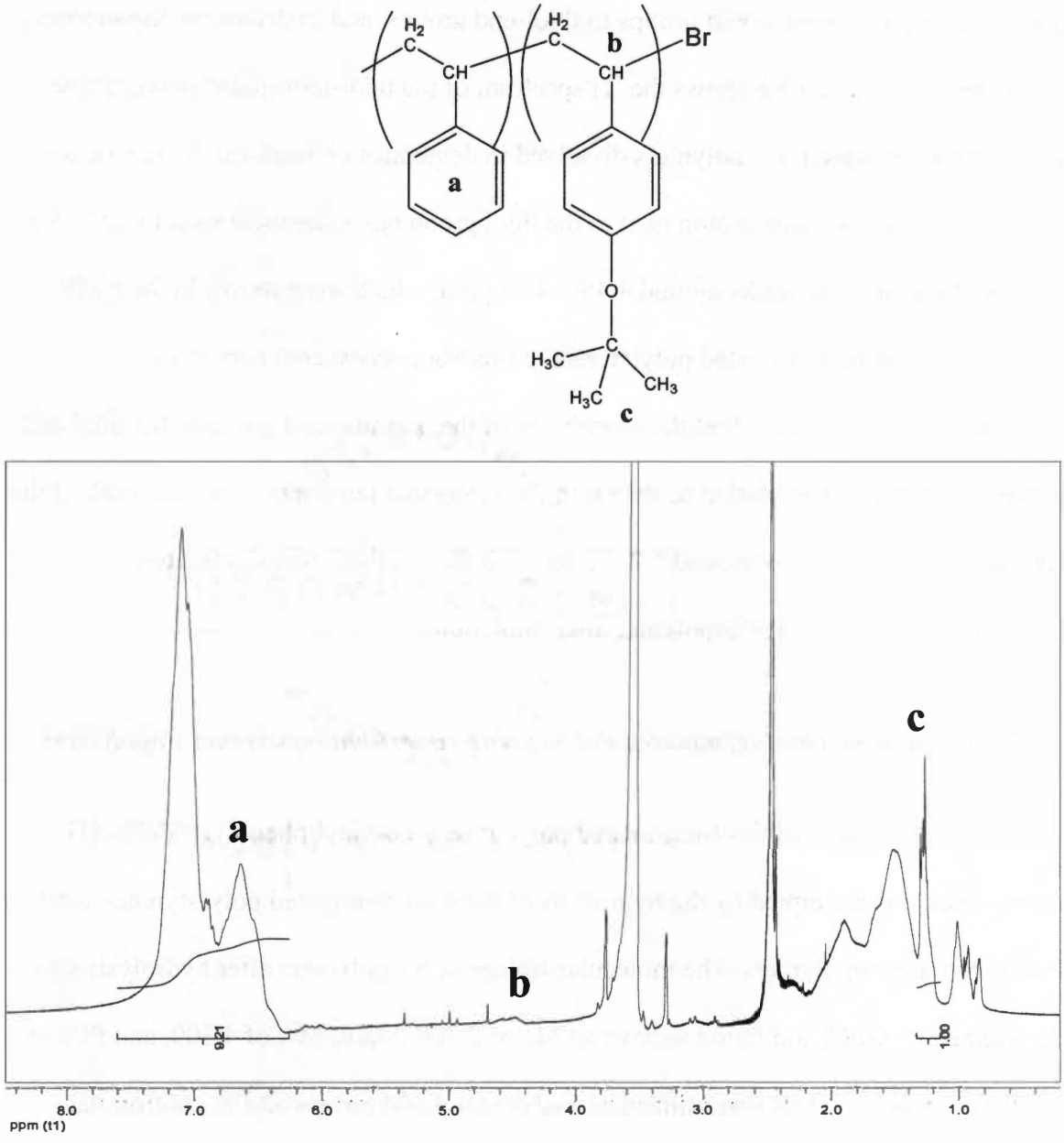

Figure 3.7 ^{1}H spectrum of bromine-terminated poly(styrene-co-4-tert-butoxystyrene) copolymers dissolved in deuterated dioxane.

the conversion of bromine-end groups to thiol-end groups, and to determine the success of this reaction. Figure 3.8 shows the ^{1}H spectrum of the thiol-terminated poly(styrene-co-4-tert-butoxystyrene) copolymers dissolved in deuterated chloroform. As can be seen in Figure 3.8, the methine proton next to the thiol group has a chemical shift of 2.9 – 3.2 ppm. Additionally, the peaks around 4.45 – 4.75 ppm, which were shown in the NMR data of the bromine-terminated poly(styrene-co-tert-butoxystyrene) copolymers, disappeared. This indicates that the conversion of the bromine-end group to the thiol end group occurred upon thiolation of the bromine-terminated polymers. Also, the peak of the tert-butoxy group protons around 1.2 – 1.4 ppm indicates there remains the tert-butoxystyrene group in the copolymer after thiolation.

3.2.7 Hydrolysis of Thiol-terminated Poly(styrene-co-tert-butoxystyrene) Copolymers

The synthesis of thiol-terminated poly(styrene-co-vinyl phenol) (PSVPh-SH) copolymers was attempted by the hydrolysis of the thiol-terminated poly(styrene-co-tert-butoxystyrene) copolymers. The molecular weight of the polymers after hydrolysis was determined by GPC, and found to have an Mn of 2,700 g/mol, Mw of 4,300, and PDI of 1.60. Additionally, NMR was utilized to analyze thiol-end groups and to confirm the conversion of the tert-butoxy groups of the polymers to hydroxyl groups. Figure 3.9 shows the ^{1}H spectrum of the copolymers after hydrolysis. As can be seen in Figure 3.9, the methine proton next to the thiol end group remains at a chemical shift of 2.9 – 3.1 ppm, which indicates that the thiol end group in the copolymers remains after hydrolysis. NMR spectrum, however, suggests that some thiol-end groups were lost during hydrolysis based on the following analysis. The integration of the peak associated with

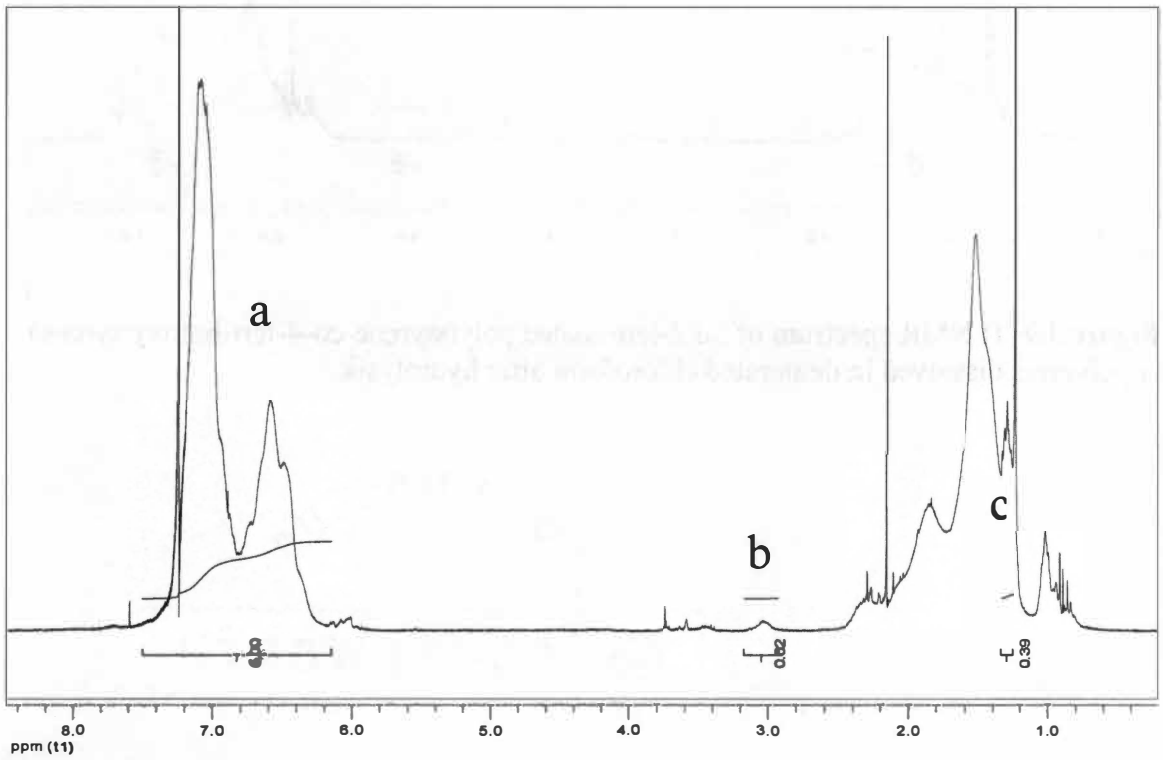

Figure 3.8 ^{1}H spectrum of thiol-terminated poly(styrene-co-tert-butoxystyrene) copolymers dissolved in deuterated chloroform.

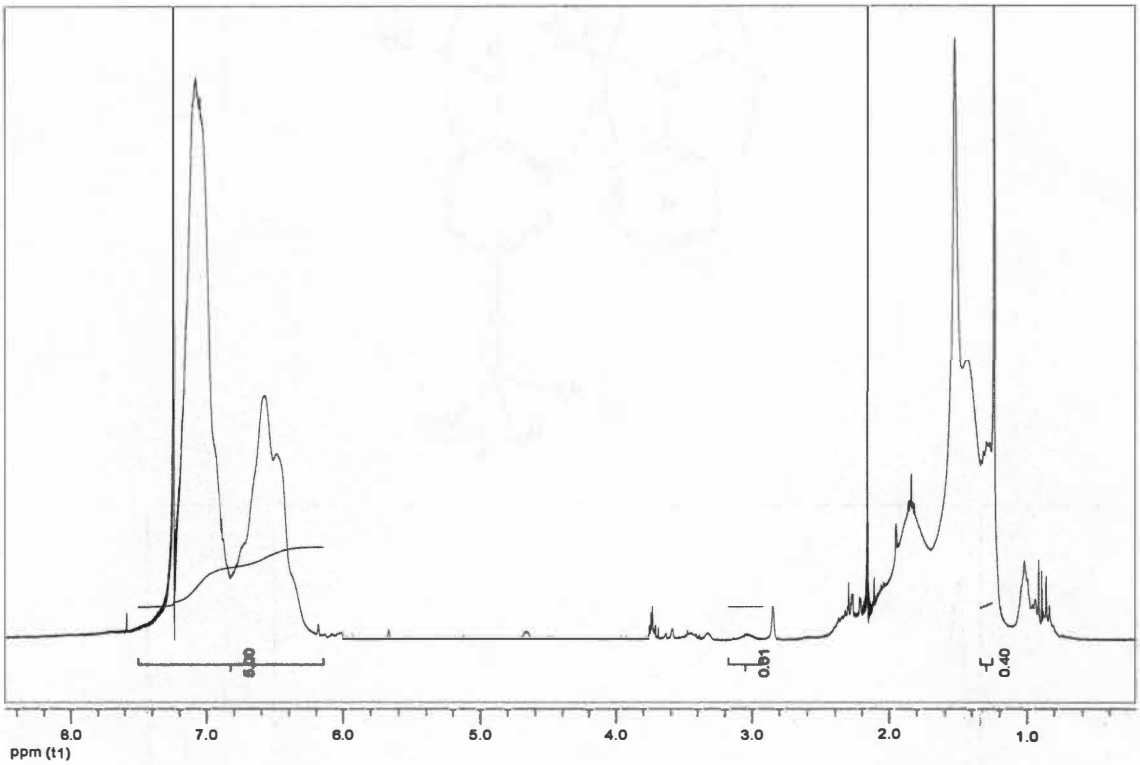

Figure 3.9 ^{1}H NMR spectrum of thiol-terminated poly(styrene-co-4-tert-butoxystyrene) copolymers dissolved in deuterated chloroform after hydrolysis.

the methine proton next to the thiol-end group provides a normalized value of $z = 0.01$. This NMR data indicates that approximately 1 end group per 100 monomers exists, or 0.01 end group per every monomer. From the molecular weight data as determined by GPC, it can be estimated that there should exist 1 thiol end group for every 30 monomers if the thiolation was successful. This correlates to $z = 0.03$ end group per monomer. Thus, this analysis suggests that some thiol end groups may be lost during the hydrolysis experiment. However, given the uncertainty in this data, more careful experiments are required to verify this interpretation of the data.

Additionally, the NMR spectrum shows that the 9 methyl protons in the tert-butoxy group at a chemical shift of 1.2 – 1.4 ppm remain, which indicates that the tert-butoxy groups still remain after hydrolysis. Also, the integration of the 9 methyl protons provide $9y = 0.40$ by normalizing the integration of all aromatic protons 5. This value (0.40) is close to the integration value of 9 methyl protons (0.39) of thiol-terminated poly(styrene-co-tert-butoxystyrene) copolymers before hydrolysis, which indicates that the conversion of the tert-butoxy group to the hydroxyl group was not successful in this study.

It is recognized that this incomplete conversion of tert-butoxy group to hydroxyl group may result of insufficient reaction time for the hydrolysis, which was only 30 mins in this study. That is, this experimental result suggests that longer reaction time for the hydrolysis may be necessary to improve the conversion of the tert-butoxy group to the hydroxyl group. Additionally, the incomplete hydrolysis may be due to an insufficient amount of HCl, which was only 5 drops in this study. However, from the NMR spectrum, it should be noted that the hydrolysis using HCl in this study may impact the thiol-end

group of the poly(styrene-co-tert-butoxystyrene) copolymers. Therefore, in future work, an efficient method to convert the tert-butoxy group to the hydroxyl group while the thiol end group remains unchanged is demanded. That is, carefully controlled reaction time and/or amount of HCl in this hydrolysis may be needed.

3.3 Conclusions

In this study, the synthesis of the starting materials to investigate sequestering surface-modified gold nanoparticles in diblock copolymers was attempted. Thiol-terminated polystyrene was synthesized starting with bromine-terminated polystyrene, followed by thiolation. Gold nanoparticles coated with low molecular weight polystyrene were synthesized by utilizing the thiol-terminated polystyrene as a stabilizing ligand. Our results indicate that low molecular weight polymers with a halogen end group can be obtained via ATRP. ^{1}H NMR spectrum shows that the thiolation of this bromine-terminated polystyrene was complete using thiourea and NaOH. The experimental results in this study also show gold nanoparticles coated with polystyrene can be synthesized, and the size of the gold nanoparticles can be controlled using this PS-SH as a stabilizing ligand. Additionally, the synthesis of thiol-terminated poly(styrene-co-vinyl phenol) copolymers was attempted starting with bromine-terminated poly(styrene-co-4-tert-butoxystyrene) copolymers, followed by thiolation and hydrolysis. Characterization results by NMR show that the thiolation of the bromine-terminated poly(styrene-co-4-tert-butoxystyrene) copolymers was essentially complete. The NMR spectrum also shows that conversion of the tert-butoxy group to the hydroxyl group by hydrolysis, however, was incomplete. NMR also indicates that the hydrolysis reaction may also result in the

loss of thiol end groups though more careful analysis is required to verify this. Increased reaction time and amount of HCl in the reaction may improve the success of the hydrolysis reaction but may impact on SH end group.

CHAPTER 4
CONCLUSIONS AND FUTURE WORK

This thesis presents experimental efforts to study the dispersion of nanoparticles in a polymer matrix using intermolecular hydrogen bonding between the nanoparticles and polymers for the purpose of controlling and realizing the tailored morphologies and thus optimizing properties of the final nanocomposites under two main topics. The first topic is the impact of sample preparation processes on the properties of polymer carbon nanotube nanocomposites. In this study, nanocomposites composed of PSVPh copolymers with 15 % mole fraction of vinyl phenol groups with either oxidized or unoxidized MWNTs prepared by three different sample preparation processes. The mechanical properties of the prepared nanocomposites were measured by DMA. Additionally, the nanocomposites were analyzed by IR to quantify the extent of intermolecular hydrogen bonding between the MWNTs and PSVPh, and to correlate the mechanical properties of the nanocomposites to the extent of intermolecular interactions between the MWNTs and PSVPh. The measured mechanical properties of the nanocomposites suggest that melt-mixing leads to more stable morphologies of the final nanocomposites than solution casting, which is probably due to the wrapping of the MWNTs with polymer chains. Additionally, the IR analysis of the nanocomposites indicates that melt-mixing can result in the formation of more intermolecular hydrogen bonding between MWNTs and PSVPh than solution casting, and thus suggests that melt-mixing can lead to the more reproducible mechanical properties than solution casting. Therefore, the DMA data and IR analysis suggest that melt-mixing is a very effective

method to prepare polymer carbon nanotube nanocomposites.

In this study, the properties of the MWNT/PSVPh nanocomposites and the intermolecular hydrogen bonding between the MWNTs and PSVPh were studied with identical MWNT and PSVPh systems. In future studies, it would be interesting to find the optimum composition of the PSVPh copolymer that maximizes intermolecular hydrogen bonding between the MWNTs and the PSVPh to realize optimum properties of the final nanocomposites. More specifically, it would be useful to study the mechanical properties of melt-mixed nanocomposites, which are composed of copolymers that contain 0 % (polystyrene), 10 %, 20 %, 30 %, and 40 % mole fraction vinyl phenol with either oxidized or unoxidized MWNTs, and to analyze the extent of intermolecular hydrogen bonding between the MWNTs and each PSVPh composition. This study will provide guidelines to maximize the intermolecular hydrogen boding between MWNTs and PSVPh. Thus, this future study will provide information on the impact of the extent of intermolecular interactions between MWNTs and PSVPh on the final morphologies of melt-mixed nanocomposites, and the impact of the final morphologies on the ultimate properties of the nanocomposites.

Additionally, in this study, the morphologies of nanocomposites were discussed based on the mechanical properties of the nanocomposites. In a future study, experimental studies that examine the dispersion of MWNTs in a PSVPh matrix would be useful to connect the morphologies of nanocomposites to the mechanical properties of the final nanocomposites. Microscopy studies of nanocomposites, such as optical microscopy can provide direct evidence of the MWNTs dispersion in a polymer matrix, or SEM provides images of the fracture surfaces of the nanocomposites and would be useful to

investigate the state of the nanocomposite morphologies in this future study.

The other topic is to synthesize starting materials to sequester surface-modified gold nanoparticles in one phase of diblock copolymer systems. The long term goal of this project is to control the morphologies of the diblock copolymer nanocomposites, and thus to realize the desired properties of the nanocomposites by investigating the impact of enthalpic attractions between nanoparticles and polymer chains in one of the blocks of the diblock copolymers on the nanocomposite structure. In this study, polystyrene-coated gold nanoparticles (PS-coated gold nanoparticles) were synthesized using thiol-terminated polystyrene (PS-SH) as a stabilizing ligand. PS-SH was synthesized by thiolation of bromine-terminated polystyrene (PS-Br), which was synthesized via ATRP. TEM images show that PS-coated gold nanoparticles can be synthesized by using the PS-SH as a stabilizing ligand, and also show that the size of the gold nanoparticles can be controlled with the PS-SH, which prevents the aggregation of gold nanoparticles.

Additionally, the synthesis of thiol-terminated poly(styrene-co-vinyl phenol) copolymers (PSVPh-SH) was attempted. This synthesis was first attempted starting with bromine-terminated poly(styrene-co-acetoxystyrene) copolymers, and followed by either hydrolysis or thiolation of the copolymers. Our experimental results indicate that the conversion of the acetoxy groups of the copolymer to hydroxyl groups and the conversion of the bromine-end groups of this copolymer to thiol-end groups were not successful. NMR data suggests that the hydrolysis of the copolymers using hydrazine hydrate results in loss of end-groups of the copolymers, and the acetoxy groups of the copolymers are not stable under thiolation using thiourea and NaOH.

Thus, the synthesis of PSVPh-SH was also attempted starting with a different

copolymer. This synthesis was attempted as follows: first, low molecular weight poly(styrene-co-4-tert-butoxystyrene) copolymers with bromine-end groups were synthesized via ATRP. Next, thiolation to convert to the end group of the copolymers to thiols was attempted. Finally, hydrolysis to convert the tert-butoxy groups to hydroxyl groups was attempted. Our NMR results indicate that the conversion of the bromine-end groups to thiol-end groups by thiolation was complete. However, the conversion of the tert-butoxy groups of the thiol-terminated poly(styrene-co-4-tert-butoxystyrene) copolymers to hydroxyl groups was not successful. Furthermore, NMR data suggests that the hydrolysis can impact the thiol-end group of the thiol-terminated copolymers. This incomplete hydrolysis is probably due to short reaction time and/or insufficient amount of HCl for the hydrolysis in this study. In future work, longer reaction time and/or sufficient amount of HCl should be attempted to complete the conversion of the tert-butoxy group to the hydroxyl group. Carefully controlled reaction time and HCl amount, however, may be needed to keep the thiol-end group of the thiol-terminated poly(styrene-co-4-tert-butoxystyrene) copolymers from being lost during hydrolysis.

The longer term goal of this project is to sequester surface-modified gold nanoparticles in diblock copolymers by incorporating enthalpic attractions between nanoparticles and diblock copolymers. That is, this system is designed such that the hydroxyl groups on the gold nanoparticles can hydrogen bond with poly(2-vinyl pyridine) (PVP) blocks of poly(styrene-b-2-vinyl pyridine) (PS-b-PVP) diblock copolymers. In future work, if PSVPh-SH is successfully synthesized, this PSVPh-SH can be used as a stabilizing ligand to synthesize PSVPh-coated gold nanoparticles. Additionally, in future work, nanocomposites composed of PSVPh-coated or PS-coated

gold nanoparticles can be prepared by solvent annealing, which is annealing a mixture of nanoparticles and polymers under a saturated solvent atmosphere.[39] To date, in most experimental results, interactions between surface-modified nanoparticles and one block of diblock copolymers in diblock copolymer nanocomposite systems are neutral. Therefore, it would be intriguing to investigate the dispersion of PSVPh-coated gold nanoparticles in PS-b-PVP diblock copolymers in that enthalpic attractions will be incorporated in this nanocomposite system. Figure 4.1 illustrates this proposed future work.

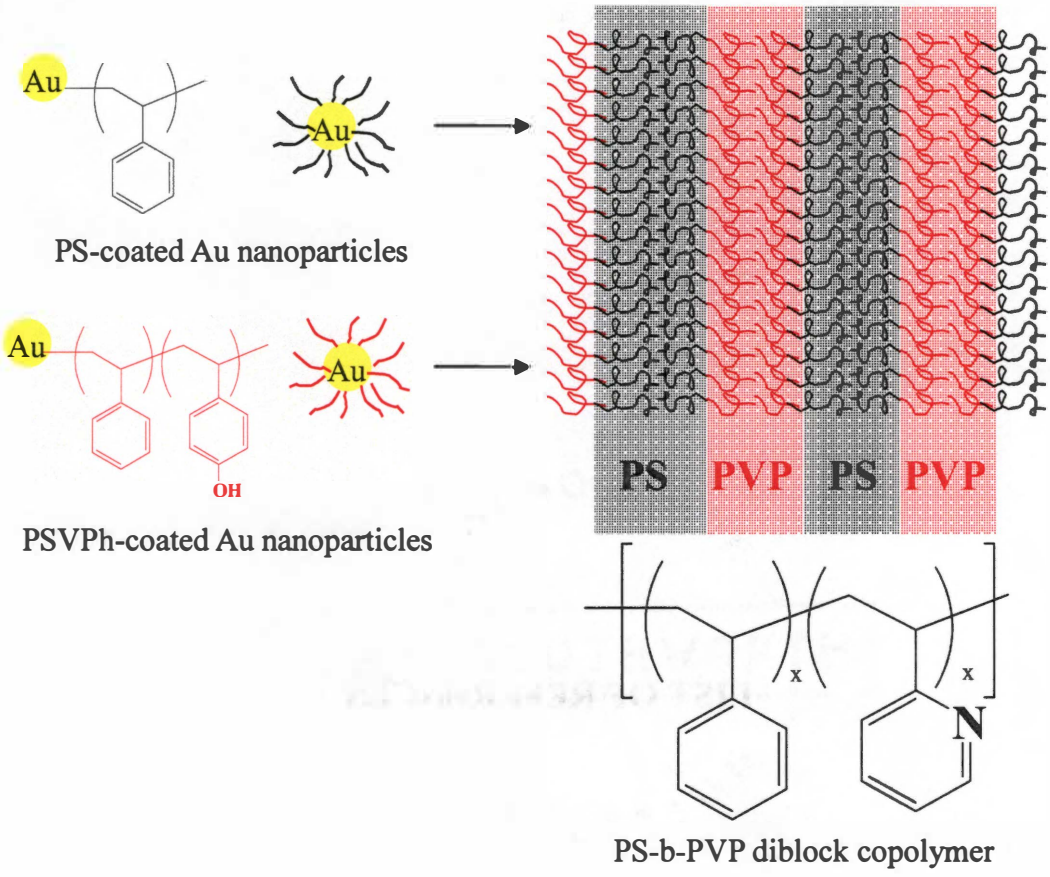

Figure 4.1 Scheme of future work for sequestering surface-modified gold nanoparticles in diblock copolymers.

LIST OF REFERENCES

LIST OF REFERENCES

(1) Fried, J. R. *Polymer Science and Technology*, Second ed.; Prentice Hall Professional Technical Reference: Upper Saddle River, **2003**.

(2) Krasteva, N.; Besnard, I.; Guse, B.; Bauer, R. E.; Mullen, K.; Yasuda, A.; Vossmeyer, T. *Nano Lett.* **2002**, *2*, 551.

(3) Balazs, A. C. *Curr. Opin. Colloid Interf. Sci.* **2000**, *4*, 443.

(4) Thompson, R. B.; Ginzburg, V. V.; Matsen, M. W.; Balazs, A. C. *Science* **2001**, *292*, 2469.

(5) Thostenson, E. T.; Li, C.; Chou, T.-W. *Compos. Sci. Technol.* **2005**, *65*, 491.

(6) Bockstaller, M. R.; Mickiewicz, R. A.; Thomas, E. L. *Adv. Mater.* **2005**, *17*, 1331.

(7) Kawasumi, M. *J. Polym. Sci., Part A, Polym. Chem.* **2004**, *42*.

(8) Okada, A.; Usuki, A. *Materials Science & Engineering: C* **1995**, *3*, 109.

(9) Bates, F. S.; Fredrickson, G. H. *Annu. Rev. Phys. Chem.* **1990**, *41*, 525.

(10) Thompson, R. B.; Ginzburg, V. V.; Matsen, M. W.; Balazs, A. C. *Macromolecules* **2002**, *35*, 1060.

(11) Tsutsumi, K.; Funaki, Y.; Hirokawa, Y.; Hashimoto, T. *Langmuir* **1999**, *15*, 5200.

(12) Zehner, R. W.; Lopes, W. A.; Morkved, T. L.; Jaeger, H.; Sita, L. R. *Langmuir* **1998**, *14*, 241.

(13) Boal, A. K.; Ilhan, F.; DeRouchey, J. E.; Thurn-Albrecht, T.; Russell, T. P.; Rotello, V. M. *Nature* **2000**, *404*, 746.

(14) Bockstaller, M. R.; Lapetnikov, Y.; Margel, S.; Thomas, E. L. *J. Am. Chem. Soc.* **2003**, *125*, 5276.

(15) Shenhar, R.; Norsten, T. B.; Rotello, V. M. *Adv. Mater.* **2005**, *17*, 657.

(16) Galow, T. H.; Drechsler, U.; Hanson, J. A.; Rotello, V. M. *Chem. Commun.* **2002**, 1076.

(17) Iijima, S. *Nature* **1991**, *354*, 56.

(18) Meyyappan, M. *Carbon Nanotubes Science and Applications*; CRC Press: New

York, **2005**.

(19) Moniruzzaman, M.; Winey, K. I. *Macromolecules* **2006**, *39*, 5194.

(20) Coleman, J. N.; Khan, U.; Gun'ko, Y. K. *Adv. Mater.* **2006**, *18*, 689.

(21) Gao, G.; Cagin, T.; Goddard, W. A. *Nanotechnology* **1998**, *9*, 184.

(22) Zhang, P.; Lammert, P. E.; Crespi, V. H. *Physical Review Letters* **1998**, *81*, 5346.

(23) Wong, E. W.; Sheehan, P. E.; Lieber, C. M. *Science* **1997**, *277*, 1971.

(24) Wu, M.-F.; Lourie, O.; Dyer, M. J.; Moloni, K.; Kelly, T. F.; Ruoff, R. S. *Science* **2000**, *287*, 637.

(25) Walters, D. A.; Ericson, L. M.; Casavant, M. J.; Liu, J.; Colbert, D. T.; Smith, K. A.; Smalley, R. E. *Applied Physics Letters* **1999**, *74*, 3803.

(26) Salvetat, J.-P.; Briggs, G. A. D.; Bonard, J.-M.; Bacsa, R. R.; Kulik, A. J. *Physical Review Letters* **1999**, *82*, 944.

(27) Uchida, T.; Kumar, S. *Journal of Applied Polymer Science* **2005**, *98*, 985.

(28) Dresselhaus, M. S.; Dresselhaus, G.; Avouris, P. *Carbon Nanotubes: Synthesis, Structure, Properties, and Applications*; Springer: New York, 2000.

(29) Liu, L.; Barber, A. H.; Nuriel, S.; Wagner, H. D. *Adv. Funct. Mater.* **2005**, *15*, 975.

(30) Zhang, W. D.; Shen, L.; Phang, I. Y.; Liu, T. *Macromolecules* **2004**, *37*, 256.

(31) Wang, S.-F.; Shen, L.; Zhang, W.-D.; Tong, Y.-J. *Biomacromolecules* **2005**, *6*, 3067.

(32) Geng, H.; Rosen, R.; Zheng, B.; Shimoda, H.; Fleming, L.; Liu, J.; Zhou, O. *Adv. Mater.* **2002**, *14*, 1387.

(33) Yang, J.; Lin, Y.; Wang, J.; Lai, M.; Li, J.; Liu, J.; Tong, X.; Cheng, H. *J. Appl. Polym. Sci.* **2005**, *98*, 1087.

(34) Qian, D.; Dickey, E. C.; Andrews, R.; Rantell, T. *Appl. Phys. Lett.* **2000**, *76*, 2868.

(35) Du, F.; Fischer, J. E.; Winey, K. I. *J. Polym. Sci., Part B: Polym. Phys.* **2003**, *41*, 3333.

(36) Rasheed, A.; Chae, H. G.; Kumar, S.; Dadmun, M. D. *Polymer* **2006**, *47*, 4734.

(37) Lee, J. Y.; Thompson, R. B.; Jasnow, D.; Balazs, A. C. *Macromolecules* **2002**, *35*, 4855.

(38) Bockstaller, M. R.; Thomas, E. L. *J. Phys. Chem. B* **2003**, *107*, 10017.

(39) Chiu, J. J.; Kim, B. J.; Kramer, E. J.; Pine, D. J. *J. Am. Chem. Soc.* **2005**, *127*, 5036.

(40) Nano-lab. http://www.nano-lab.com/

(41) Rasheed, A. *The Role of Specific Interactions on the Dispersion and Properties of Carbon Nanotube-Polymer Nanocomposites*, Ph. D. Dissertation, University of Tennessee, Knoxville, **2006**.

(42) Baskaran, D.; Mays, J. W.; Bratcher, M. S. *Chem. Mater.* **2005**, *17*, 3389.

(43) Stevens, M. P. *Polymer Chemistry an Introduction*, Third ed.; Oxford University Press: New York, **1999**.

(44) Pavia, D. L.; Lampman, G. M.; Kriz, G. S. *Introduction to Spectroscopy*; Harcourt College Publishers: Philadelphia, **2001**.

(45) McNally, T.; Potschke, P.; Halley, P.; Murphy, M.; Martin, D.; Bell, S. E. J.; Brennan, G. P.; Bein, D.; Lemoine, P.; Quinn, J. P. *Polymer* **2005**, *46*, 8222.

(46) Coleman, M. M.; Graf, J. F.; Painter, P. C. *Specific Interactions and the Miscibility of Polymer Blends*; Technomic Publishing Company Inc.: Lancaster, **1991**.

(47) Li, D.; Brisson, J. *Polymer* **1998**, *39*, 793.

(48) Garamszegi, L.; Donzel, C.; Carrot, G.; Nguyen, T. Q.; Hilborn, J. *Reactive & Functional Polymers* **2003**, *55*, 179.

(49) Daniel, M.-C.; Astruc, D. *Chem. Rev.* **2004**, *104*, 293.

(50) Brust, M.; Walker, M.; Bethell, D.; Schiffrin, D. J.; Whyman, R. *J. Chem. Soc., Chem. Commun.* **1994**, 801.

(51) Bockstaller, M.; Kolb, R.; Thomas, E. L. *Adv. Mater.* **2001**, *13*, 1783.

(52) Asari, T.; Matsuo, S.; Takano, A.; Matsushita, Y. *Polym. J.* **2006**, *38*, 258.

(53) Wang, Z. L. *Part. Part. Syst. Charact.* **2001**, *18*, 142.

(54) Ohno, K.; Ejaz, M.; Fukuda, T.; Miyamoto, T.; Shimizu, Y. *Macromol. Chem. Phys.* **1998**, *199*, 291.

VITA

Chang-Uk Lee was born in Busan, South Korea on February 24th, 1976. He graduated from Hyekwang High School in Busan in 1994. He attended Pusan National University in Busan, South Korea, and received a Bachelor of Science degree in 2004 with a major in Polymer Science and Engineering. He then joined the graduate program in the Materials Science and Engineering Department at the University of Tennessee, Knoxville in August, 2004. He started graduate research as a research assistant in the Chemistry Department under the direction of Professor Mark Dadmun in January, 2005. He successfully defended his Master thesis in November, 2006, and received a Master of Science degree with a major of Polymer Engineering in the Materials Science and Engineering Department in December, 2006.

5873 8921 3
04/04/07 VR
HGroup